SINGLE-CELL-BASED INVESTIGATION OF HL60 DIFFERENTIATION USING A MICROWELL ARRAY

A Thesis

Presented to the Faculty of the Graduate School

of Cornell University

in Partial Fulfillment of the Requirements for the Degree of

Master of Science

by
Lina Moufid Aboulmouna
May 2015

ABSTRACT

The average cell population response to a range of stimuli inaccurately reflects individual cell response due to heterogeneity in previously assumed homogeneous cell populations. It is hypothesized that this contributes to metastatic potential in tumors, with the most invasive cells being molecularly and behaviorally distinct from the bulk. In the work presented here, we designed and optimized a microwell array for use in high throughput single cell studies with the ultimate goal of studying heterogeneity in tumor populations. We investigated device shape, seeding density, and well depth, diameter, and spacing. The acute myeloid leukemia cell line HL60 was used as a model uncommitted precursor cell line and we began investigating population variance by inducing differentiation along the granulocytic lineage with all-trans retinoic acid (ATRA).

BIOGRAPHICAL SKETCH

Lina Aboulmouna grew up in the hills of middle Tennessee in the small town of Tullahoma. Lina graduated valedictorian of her class from Tullahoma High School in 2007 and continued on to her birthplace where she attended Vanderbilt University in the heart of Music City Nashville, Tennessee. In 2011, Lina completed her Bachelor of Engineering degree from Vanderbilt University in Chemical Engineering with a biotechnology focus and minors in mathematics and chemistry. In 2011 she was awarded a National Science Foundation Graduate Research Fellowship (NSFGRF) to pursue her graduate studies in Chemical and Biomolecular Engineering.

To those whom have encouraged me and have recognized my full potential well before I ever did,

in particular my teachers and coaches…

ACKNOWLEDGEMENTS

I would first like to thank my research advisers, Dr. Jeffery Varner and Dr. Abraham Stroock. Both have been supportive and committed to helping me become a successful researcher and have provided me with many helpful resources and insights into my project. I would also like to thank individuals in the NanoBioTechnology Center and Cornell Nanoscale Facility that helped train me on the necessary tools and procedures as well as provided general support throughout the progress of my work, specifically Penny Burke, Teresa Porri, and Michael Skvarla. I would also like to thank my Stroock and Varner lab mates and my peers who have provided me positive and stimulating discussions on my project, especially Mengrou Shan, Dr. Russell Gould, and Dr. Holly Jensen. Furthermore, I would like to thank all of my family (Nada, Moufid, Ziad, Lora, and Lorina Aboulmouna) and friends around the world who have provided me with love and support in recent years, including my "families" in Ithaca, who have adopted me as one of their own: Steven and Sheryl Froehlich, Dr. Theodore and Angele Lowi, their children Anna and Jason, and their dogs Bix and Mr. Skeffington. I would like to extend that gratitude to my undergraduate research advisor and mentor Dr. Jamey Young, and friends Stephen Schumacher, Lauren Mitchell, Lara Jazmin, Dr. Ashwana Fricker, Peter DelNero, Casey Garland, Olufunmilayo Adebayo, Dr. Anne Rocheleau, John Foo, especially Ashley Kaminski, Gregory Fedorchak, and Maria Carpintero Torres-Quevedo for the countless hours of their energy, time, and love poured onto me that constantly amazes me, and most importantly, the friend who has been by my side unconditionally the past year, my dog Buddy.

TABLE OF CONTENTS

LIST OF FIGURES

LIST OF TABLES

CHAPTER 1

INTRODUCTION

Measurements of biochemical processes are crucial to the development of predictive computational models in human health and development. High-throughput single-cell measurements of cellular responses are of great importance for a variety of applications within basic cell biological signaling networks and, in particular, to create model parameters for predictive purposes [1-3]. Determining multiple biochemical parameters of single cells in parallel provides information for the generation of a parameter ensemble, ultimately allowing for the development of new insights into cell-cell signaling [4-6]. This is important because the measurement of cell population averaged response to a stimulus has been shown to inaccurately reflect individual cell responses due to heterogeneity among previously assumed homogeneous cell populations [7-9]. Population heterogeneity is consistent with the observation of primary epithelial tumor cells, in which the most invasive cells are found to be molecularly and behaviorally distinct from those in their bulk tumor cell environment [10]. Strikingly, significant cell-to-cell variation has also been observed in presumably uniform populations like clonal cell lines due to a natural consequence of positive feedback in the mechanisms controlling gene expression [11,12].

Applying single cell analysis to study behavior of tumor cells is becoming increasingly important, especially in understanding metastasis – the leading cause of cancer related deaths (~90% of cancer progresses to metastatic stage) [13]. Solid tumors contain diverse subpopulations of cells that result from a number of root causes such as genetic instability, microenvironment

selectiveness, and surrounding phenotypic drives. This sort of diversity results in vast heterogeneity within tumor cells which leads to obstruction in our understanding of cancer and its treatment. Understanding how malignant tumor cells spread from a primary tumor to form a secondary tumor is critical in understanding cancer progression and its regulation [14-17].

One approach which allows for study of both individual and collective cell response and behavior involves the use of microwell arrays. ***The goal of this study is to design, optimize, and perform proof of principle experiments of a microwell array platform to enable single cell capture and analysis***. We address cell-cell heterogeneity within proof of concept experiments using the human myeloid leukemia cell line HL60 and demonstrate the need for single cell analysis as we begin to study the heterogeneity in differentiation promoted by all trans retinoic acid (ATRA) [18]. We intend to expand our applications to include circulating tumor cells, which are malignant cells released from the primary tumor cite and disseminate to distant cites via the blood stream or lymphatic system [19]. Single cell analysis studies provide opportunity for addressing these heterogeneous cell populations without the added complexity and diversity of cells found within the tumor environment that may mask leading cell responses that could lead to an understanding of the metastatic process of cancer [20].

CHAPTER 2

BACKGROUND AND LITERATURE REVIEW

This project is founded on knowledge of current single cell analysis approaches as well as an understanding of the HL60 cell line that is used to validate our device. Single cell methodologies are a hot topic in the stem cell field and in cancer research. Since this device was motivated by a desire to study tumor heterogeneity, background information on metastasis, epithelial-to-mesenchymal transition, and circulating tumor cells is included briefly.

2.1 Motivation for Single Cell Studies

Variation observed at the cellular level is closely linked to the stochastic nature of underlying biological systems [21]. Cellular networks are inherently noisy, displaying a distribution of gene expression across cells even under identical environmental conditions. We can model this natural distribution using stochastic simulation. For example, high-throughput measurement of gene expression combined with systematic perturbation of environmental or cellular variables provides information that can be used to generate novel insight into the properties of gene regulatory networks. Studies of ion channels, signaling pathway dynamics, and transcription factor networks have shown that the behavior of a cellular system is often much more stochastic and discrete than would be assumed from population averages. At the level of individual molecules, and even single cells, biological processes tend to have probabilistic rather than continuous response curves and undergo rapid shifts between metastable states [22-24]. What appear to be smooth transitions at the bulk-cell level may be anything but smooth at the individual level. These issues can pose a serious challenge for traditional experimental

approaches that rely on bulk cell assays because the average values obtained may not actually be representative of any given cell in the population [25-27]. The goal of this project is to develop an approach to produce high-throughput, single-cell measurements that will greatly increase the accuracy, content, and statistical power of the collected biological data.

2.2 Cytometry approaches

Traditionally, flow cytometry (FC) has been the tool of choice for fluorescence-based assays at the single cell level. FC is a well established technique that can provide single-time-point measurements of multiple parameters, including cell size, count, and granularity of entire cell populations [28]. The most widely used clinical applications of FC are in the classification of hemopoietic cells by cell surface immunofluorescence [29]. Although a very powerful tool, FC has a few limitations that hinder its use in specific applications. FC is limited by the need to keep cells in suspension and the inability to track individual cell properties through time. Analysis of solid tissue by FC is based on measurements of dissociated cells or nuclei, and the isolation procedure has a tendency to produce a number of undesirable effects. For instance, the effects of the extracellular environment on cell behavior (e.g., relationship of tumor cells to the host stromal or infiltrating cells) may be lost or distorted during the FC preparation, which involves dissociating cells from their matrix or substrate [28-30]. Additionally, FC is unsuited for time resolved studies of single cells because restaining of the cells after the initial measurement is not possible [30]. Looking to the future applications of this device, such as circulating tumor cell (CTC) detection, there are specific limitations. The surface markers used to identify CTCs may vary depending on the origin of the CTC and the stage of differentiation it has undergone [29].

However, a specialized type of FC sorting is fluorescence-activated cell sorting (FACs), which may be useful for CTCs although it does not overcome the previously mentioned limitations [28].

Image cytometry has become a viable alternative to conventional FC with detection modalities, rapid increases in computational power, and the development of better analysis techniques [31]. Image cytometry is a range of methods by which microscopic images deduce quantitative biological information. A number of thorough image processing steps, e.g. subtraction, filtering, thresholding, pixel averaging, and background subtraction, are often found in image collection to differentiate target cells from background material [28, 30]. One way to reduce this procedural complexity is by better controlling the spatial arrangement of the cell population being studied. Much of the difficulty in image cytometry comes from interpreting random seeding patterns and identifying cell boundaries. These issues can both be addressed by controlling for cell density. However, unlike in FC, photobleaching is a concern due to prolonged integration times and exposure of cells to fluorescence.

Laser scanning cytometry (LSC) is another method that can be used for cellular imaging using the combined flow and image cytometry techniques already discussed. LSC offers few of the limitations that are available in its counterparts and contains even more advantages. However, the key attribute of LSC that differentiates it from FC is the use of a slide for visual examination and measuring cells over a period of time. The accuracy and sensitivity of cell fluorescence measurements by LSC are comparable to the most advanced flow cytometers [29, 30]. However, LSC measures individual pixel values. Relocation of cells after measurement, minimal cell loss during preparation and staining of the sample, and the indefinite storage of cells once analyzed

are advantages of LSC that drastically reduce the required sample size. Despite these strengths, LSC is performed for time resolved events limited to time resolutions of 10 to 60 seconds [30]. Another approach, and one we focus on, allows for prolonged cell analysis of hours to days which involves the physical entrapment of individual cells in microwell arrays.

2.3 Microwell Devices

High density microwell arrays combined with integrated alignment and identification features simplify the image processing needed for effective image cytometry. For example, with microwell arrays we can study the same cell across multiple time points. Given our interest in measuring cell response over the course of hours to days, the previously defined methods do not satisfy our needs due to increased cell sample photobleaching with prolonged exposure. Microwell arrays can allow for thousands of cells to be tracked across multiple time points, even when the devices undergo significant manipulation between measurements [9, 11, 12, 31-34]. Previous studies prove microwell arrays are a useful technological tool implemented for a number of different applications [35-39]. In the following sections, we elaborate upon some of these applications.

Circular microwell arrays

Embryonic stem (ES) cells are characterized by their ability to differentiate into specific tissue lineages depending on the temporal and spatial intrinsic and extrinsic signals they receive. Moeller *et al.* created a microarray platform to study the behavior of ES cell proliferation and homogeneity in a controlled microenvironment using a number of different materials in a microwell format [35]. Using photolithography techniques, a chrome etched mask with patterns

of circular microwells with 50 μm, 75 μm, 100 μm, 150 μm, and 175 μm diameters was created on negative resist SU-8 coated silicon wafers, and the non-exposed regions of the resist were developed away to create the masters. Poly-dimethyl-siloxane (PDMS) molds were cured on a silicon master. The PDMS stamp was then placed on an evenly distributed film of PEG monomer solution and photocrosslinked. ES cell differentiation is affected by microenvironmental stimuli that directly or indirectly depend on embryoid body (clusters of ES cells) size (Figure 2.1).

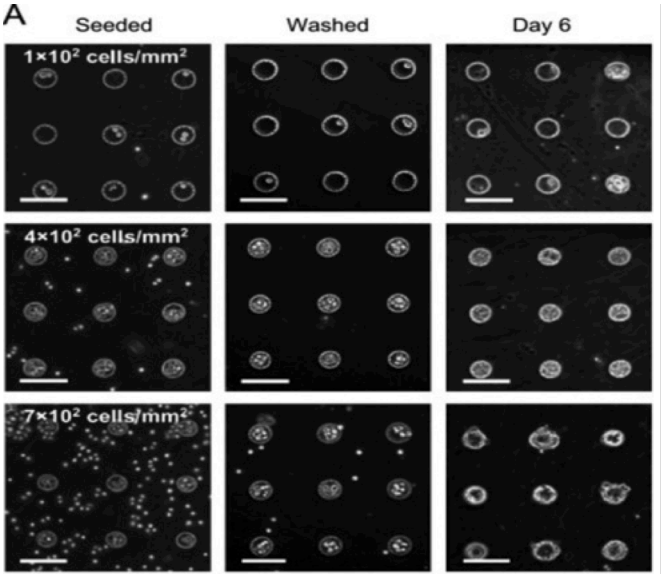

Figure 2.1 Microwell array for growth of embryoid bodies and stem cells designed by Moeller *et al*. [35]

Environmental stimuli influences cell–cell, cell–extracellular matrix (ECM), and cell–soluble factor interactions as well as environmental and physicochemical factors including temperature, pH, and oxygen availability. Since these parameters tend to be functions of embryoid body size, cell populations obtained from suspension cultured embryoid bodies can vary dramatically—even when they were cultured under identical conditions. To uniformly direct embryoid body and consequently ES cell differentiation, microenvironmental stimuli must be precisely controlled by homogenizing the embryoid parameters, in particular, size and shape [35].

Another circular patterned microwell array device developed by Motler *et al.* is designed to measure single cell oxygen consumption rate (OCR). Motler *et al.* used photolithography techniques to create a chrome and gold etched photomask [36]. Using this photomask, exposed glass is etched away in 49% hydrofluoric acid (HF) to a depth of 25 µm. Each fabrication produces thirty-two 1 cm by 1 cm chips per wafer with each chip containing 16 microwells. The dimensions of a microwell within this array were: diameter of 65 µm, depth of 25 µm, volume of 80 µL, and spacing between wells of 235 µm. Each microwell contained a phosphorescent oxygen sensor attached along the well inner base circumference. The microwell array platform was tested with four cell lines originating from macrophage, epithelial lung cancer, and esophagus seeded at a concentration to yield 1 to 2 cells per well (Figure 2.2). The OCR variations that were observed between the cell types reflected the different metabolic rates of the different cell lines [36].

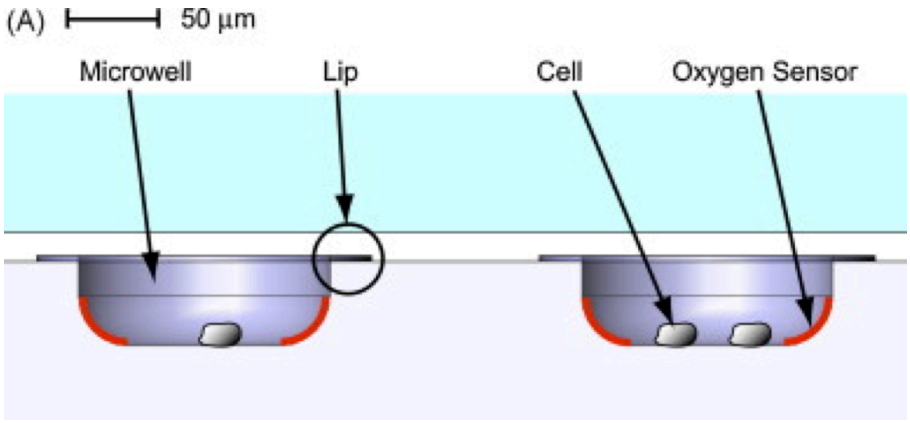

Figure 2.2 Oxygen sensing microwell construct developed by Motler *et al.* [36]

Honeycomb/Hexagonal microwell arrays

The cell retainer (CR) developed by Deutsch *et al.* enables repetitive, high-content signal and image analysis of the same non-adherent, non-tethered individual cells or groups of cells, being subjected to various bio-manipulations and staining [37]. The CR is arranged in hexagonal wells, with 8 μm depth and 20 μm pitch made of glass, in a densely compact honeycomb-like pattern. The edges of the walls are extremely sharp, forcing precipitating cells to settle inside the wells rather than in between (Figure 2.3). The honeycomb-like pattern was created using a photoresist coating on the chrome coated glass mask and then developed away. The glass mask acting as its own substrate was then etched with HF acid until the desired geometry and surface quality is obtained. The well setup allows for repetitive dynamic measurements of the same individual non-adherent cells within a population including functional, post-fixation, and molecular data obtained on the same individual cell [37].

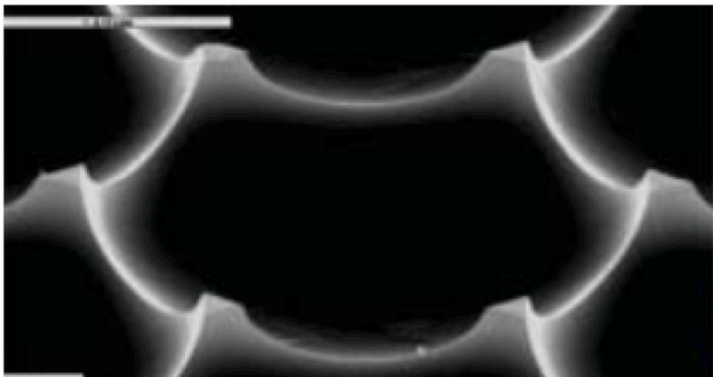

Figure 2.3 Scanning electron micrograph image of the Cell Retainer structure, scale bar: 10 μm [37].

Work done by Meek *et al.* also involved a hexagonal well design incorporating a thin protein layer of avidin-biotin complex within each microwell [38]. Avidin is a tetramer with four identical subunits each of which is capable of binding one biotin. The biotin–avidin complex is practically unaffected by pH, temperature, organic solvents, and other denaturing agents. As a

result, countless biomolecules can be coupled to biotin with minimal loss of activity. Microwell array fabrication involved polishing and chemically etching an imaging fiber's distal face composed of ~ 3000 count imaging fibers each comprised of ~ 22 μm wide hexagonal cores. The polished distal imaging fiber face was suspended and sonicated in the HF-etching solution to obtain the desired well depth of 1–14 μm, ~ 22 μm wide, flat-bottomed wells with ~ 5 pL volumes. However, this patterned approach limits device characteristics to fixed parameters except for the well depth (Figure 2.4) [38].

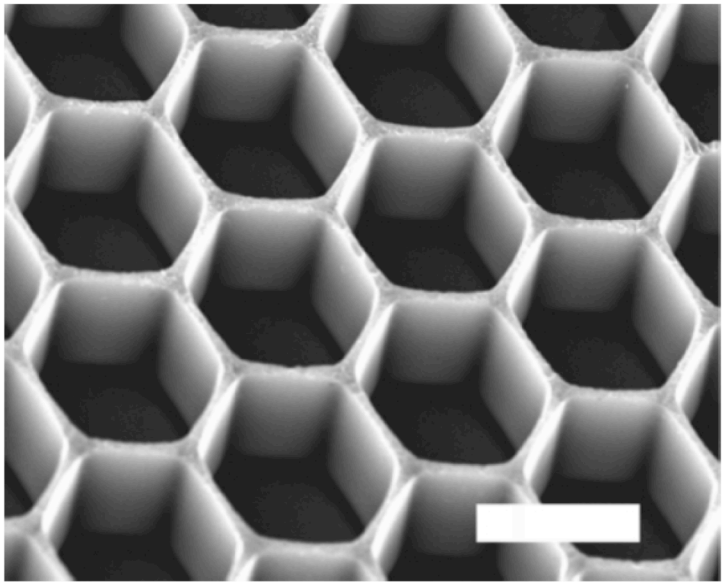

Figure 2.4 Scanning electron micrograph of a region of a ~3000 count microarray, scale bar: 20 μm [38].

Square microwell arrays

In the work done by Love *et al.* successful selection and isolation of hybridomas were performed using their developed microengraving technique [39]. The process involves screening of antibodies produced by large numbers of cells and retrieving those cells that produce antibodies of desired specificity. Photolithography and replica molding techniques were used to fabricate poly-dimethyl-siloxane (PDMS) microwell arrays. A positive relief photomask was used to

pattern a SU-8 coated silicon wafer and then developed away to produce the positive relief pattern on the wafer. PDMS was then cast and cured on the master to produce the device pattern consisting of square well dimensions of 50 μm separated by 50 μm or 100μm separated by 100 μm with a well volume of ~0.1-1 nL. Once cells were loaded onto the device at a concentration of ~$1x10^5$ to $5x10^5$ cells/mL, an epoxide-functionalized glass coverslip with immobilized secondary antibody was incubated with the microwell array wells facing down on the slides (Figure 2.5). This microengraving technique requires that the cell line of study secrete an antibody of interest. The primary antibody is then captured from cells contained in the microwells onto the glass slide which is then removed and stained with a fluorescently labeled secondary antibody. Correlating the region of microwells on the PDMS slab with the matching region of the microengraved glass cover provides information given the specificity of the antibody produced by the individual cells within each well [39].

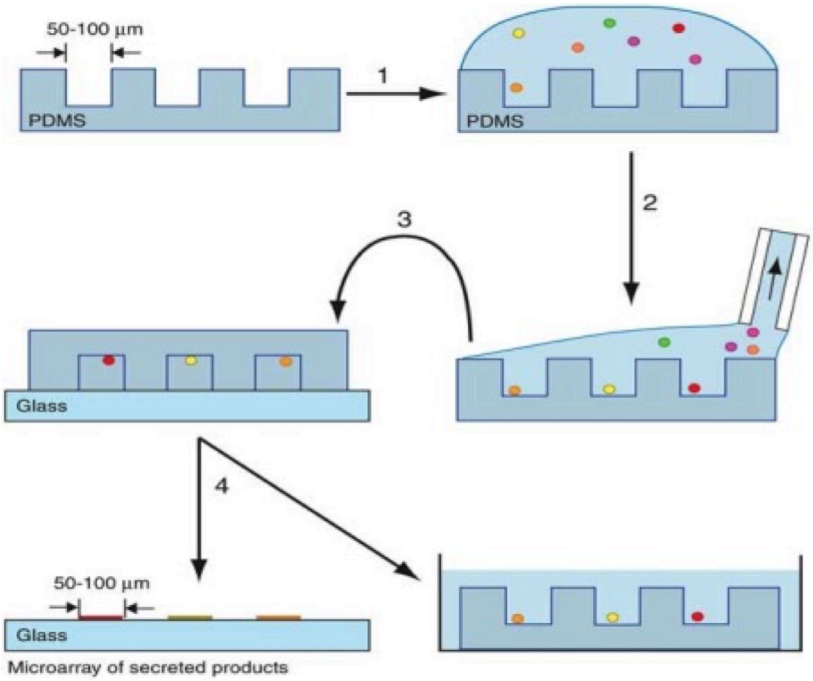

Figure 2.5 Microengraving technique setup designed by Love *et al*. [39]

Adapting the Microwell Array Platform

Microwell arrays are an emerging cell culture and imaging platform that allow for high-throughput single cell analysis, yet require very little effort to reproduce once designed using photolithography or replica molding techniques. The platform design used for this study pulls from many of the methods cited previously. In particular, using photolithography techniques, we adopt the square well pattern used by Love *et al.* due to ease as well as reduction in cost and time to produce a chrome etched photomask with square rather than circular or hexagonal wells. To create our wells however, we chose to use an etch process rather than spin coat SU-8 photoresist onto a silicon wafer in order to provide better resolution and consistency in our well depth from device to device and within each device. As was examined by Moeller *et al.*, we also explore multiple parameters including depth, width, and spacing to optimize our device for single cell study using HL60. We use this non-adherent cell line to optimize and perform proof of principle experiments with our device design.

2.4 HL60 as a model uncommitted precursor cell line

HL60 cells are derived from a patient with acute promyelocytic leukemia and have been used for experimental systems since the late 1970s [15-18]. Most myeloid leukemia cells when cultured in liquid suspension undergo a limited number of cell divisions prior to growth arrest and cell death, whereas HL60 cells continuously proliferate in conditioned media with a doubling time of 36 to 48 hrs [15]. Relatively few human leukemic cell lines displaying distinct myeloid or myelomonocytic characteristics have been established [18]. The most interesting feature researchers focus on is the capacity of HL60 to differentiate *in vitro* to a variety of different cell types of the myelomonocytic lineage. HL60 cells are bipotent myelomonocytic precursors,

capable of being induced to terminally differentiate into four general types of cells: (a) granulocytes, (b) monocytes, (c) macrophagelike cells, and (d) eosinophils [15-18, 40]. These category designations are somewhat arbitrary and certain HL60-inducing agents give rise to cells with overlapping characteristics [40-43].

Induced Differentiation in HL60

Nevertheless, these categories provide a convenient outline for discussing the numerous and complex phenotypic changes induced in this leukemic cell line by a wide variety of agents. For example, treatment with all-trans retinoic acid (ATRA) induces differentiation of HL60 along the granulocytic lineage into neutrophil-like cells and is most pertinent to this study. Other compounds like 1,25-dihydroxyvitamin D_3, (VD3) 12-O-tetradecanoylphorbol-13-acetate (TPA), and granulocyte/macrophage colony-stimulating factor (GM-CSF)—potent growth factors stimulating the development of various lineages of hemopoietic cells—can induce HL60 to differentiate to monocytic, macrophage-like, and eosinophil phenotypes, respectively [41, 44-47].

All-trans retinoic acid induced differentiation

At least a 12-hour exposure to DMSO or retinoic acid is necessary before any differentiation occurs and continuous exposure to these compounds is generally required to induce maximum differentiation [18, 40]. ATRA induces differentiation (as measured morphologically and by the ability to reduce nitroblue tetrazolium) of HL60 at concentrations as low as 1 nM with maximal differentiation (approximately 90%) occurring at 1 μM. The continuous exposure to retinoic acid is necessary for optimal differentiation, with the percentage of mature cells in the culture directly related to the length of time of exposure to retinoic acid [16-18, 40-42]. The ability of retinoic

acid to convert proliferating HL60 leukemic promyelocytes to terminally differentiated, functionally mature granulocytes suggests that this compound could provide a therapeutic tool in the treatment of acute myeloid leukemia, a disease that has been viewed as the primary block in myeloid differentiation [40].

Adopted cell model

Due to its robust qualities and relevance to disease progression of leukemia *in vivo*, we use HL60 as a model cell line to layout the foundation of work done on our microwell array for single cell analysis. We started with the stimulus first mentioned: all-trans retinoic acid—a vitamin A derivative—to look for differentiation of the treated cells into granulocytic cells [16-18, 40-42]. Treatment of HL60 with ATRA in the context of a single cell study could provide valuable information on the differentiation mechanism of HL60 *in vitro* and could be translated to reflect *in vivo* conditions.

The ultimate goal of this work is to be able to study and model the stochastic nature of cancer metastasis, and specifically the dissemination of circulating tumor cells (CTCs) from primary tumor to secondary tumor cite. Although the below information is not directly relevant to the work presented here, it is the primary motivation behind the project and is presented to provide a scope of the future work and applications.

2.5 Metastasis

Understanding metastasis and the molecular signature of the cells that are able to undergo the process is essential for understanding how to prevent cancer related deaths. The process of

metastasis involves a series of sequential steps (Figure 2.6) in which malignant cells are released from the primary tumor cite and disseminate to distant cites via the blood stream or lymphatic system. An important question that has arisen is whether these initiating cells are cancer "stem cells". Direct support for the existence of cancer stem cells in carcinoma has come from mouse models of epithelial tumorigenesis and from preliminary patient data [50]. However, some studies suggest that tumors are not necessarily initiated by rare cancer stem cells but rather that a significant percentage of individual human melanoma cells can efficiently form these tumors [51, 52]. Population heterogeneity is consistent with the observation of primary epithelial tumor cells, in which the most invasive cells are found to be molecularly and behaviorally distinct from those in their bulk tumor cell environment [10]. The resulting prognosis for diseases such as luminal breast cancer typically have a lower associated risk of metastasizing, but even then there is still an 8-10% chance in which collective invasion of functionally distinct epithelial cells within the tumor transitions to a motile phenotype occurs via cell-cell interactions. This process by which cells migrate from an epithelial stationary phenotype to a motile mesenchymal phenotype is termed epithelial to mesenchymal transition [53, 54]. Data also indicates that EMT may not only be necessary for primary carcinoma to invade and disseminate, but also that these pioneer invasive cells with both a mesenchymal and a stem cell-like phenotype can generate a differentiated epithelial-like structure by a reverse process mesenchymal to epithelial transition (MET) [55-57].

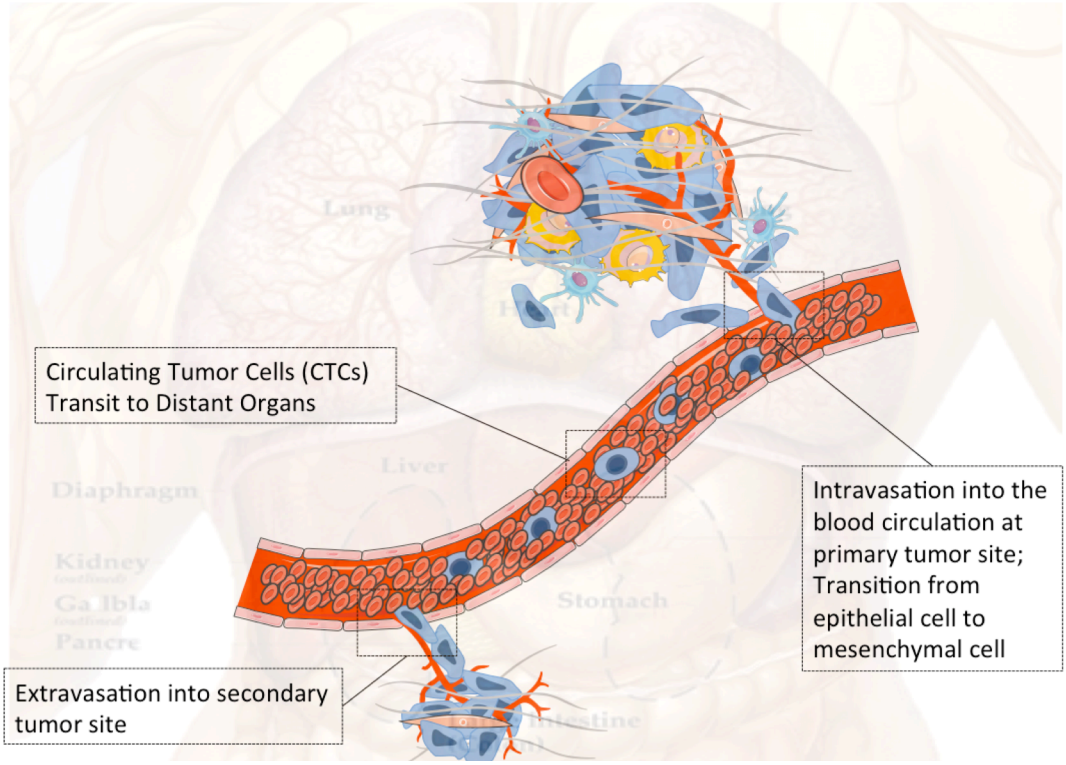

Figure 2.6 Dissemination of metastatic tumor from primary tumor site to secondary tumor site.

Blood vessels within tumors offer a critical entry point for malignant cells to enter into the blood stream via intravasation. Circulating tumor cells are the intermediate step between when a cell has undergone EMT from the primary tumor site entering into the vascular system and prior to the extravasation of the mesenchymal cell back into epithelial tissue to form the secondary tumor site [54, 58-60].

Circulating Tumor Cells

Tissue invasion can start as early as initial tumor development in the primary tumor site (Figure 2.6) [15, 16, 56-58]. Detection, monitoring and molecular analysis of circulating tumor cells (CTCs) may provide a non-invasive approach to the detection of early tumor dissemination and the assessment of prognosis and appropriate treatment for established cancers [59, 60]. CTCs

identical to those in primary tumors were first discovered by Ashworth in 1869 and were later regarded as a hallmark of the 'leukemic phase' of cancer [61]. CTCs have since been the subject of an increasing number of clinical studies; however, identifying cancer cells (typically 3-5 cells) among over 100 million leukocytes and 50 billion erythrocytes found in normal blood cells is challenging during the early stages of cancer. In recent years, many new methods have been developed to enrich and detect these rare CTCs in peripheral blood [62, 64]. The different technologies involved, coupled with the heterogeneity of the screened populations, make the clinical significance of CTCs difficult to interpret [62-65].

Concern that CTCs are not properly or consistently identified is supported by immunohistochemical studies suggesting that up to 20% of breast cancers do not express EpCAM [66]. Expression of EpCAM, an endothelial cell marker, is consistently used as an identifier of CTCs. Indeed, expression of EpCAM may be related to the intrinsic biologic cancer subtype, and, furthermore, cancers may lose EpCAM expression during the metastatic process in their transition to mesenchymal cell types [54, 63]. Studying individual cells and their behavior through transition in response to stimuli can provide for more relevant information on future assessment and identification of CTCs.

CHAPTER 3

METHODS

3.1 Device Formulation

3.1a Device design

For the purpose of studying hundreds of individual cells in a single experiment, a microwell array platform was chosen for the device framework. We fabricated arrays of microwells by a combination of photolithography and poly-dimethyl-siloxane (PDMS) replica molding. The microwell arrays were either 50 μm or 100 μm in diameter (Figure 3.1.B). Various well depths (30 μm, 50 μm, or 100 μm) and spacings (50 μm, 100 μm, 150 μm, or 300 μm) were also tested (Figure 3.1.C, Figure 3.1.E). Combinations of these parameters were tested in order to arrive at the optimal design for single cell studies. Each PDMS slab contained a square array of 40 by 40 wells. Figure 3.1 illustrates the device with the PDMS component (Figure 3.1.A) sitting directly on a glass slide enclosed within the confines of a polycarbonate imaging apparatus.

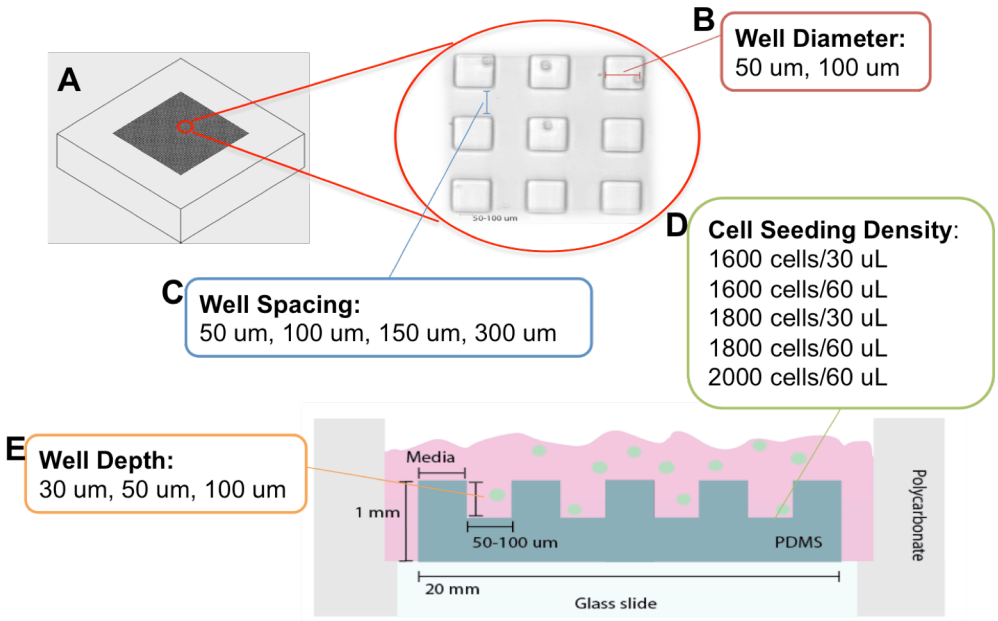

Figure 3.1 Illustration of device parameters. The parameters evaluated were (A) device shapes of circular disks and square slabs, (B) well diameters of 50 µm and 100 µm, (C) well spacing of 50 µm, 100 µm, 50 µm, and 300 µm, (D) five cell seeding densities of 1600 cells/30 µL, 1600 cells/60 µL, 1800 cells/30 L, 1800 cells/60 µL, and 2000 cells/60 µL, finally, (E) well depths of 30 µm, 50 µm, and 100 µm.

3.1b Microwell array master fabrication

As depicted in Figure 3.2.1-8, we fabricated the microwell array using standard photolithography techniques. A positive tone (dark field) chrome etched photomask was made from a pattern containing device designs generated using Autodesk's AutoCAD software package. A 1.3 µm layer of positive photoresist (Series 1813) was spun at 5000rpm for 30 seconds onto a 4 inch silicon wafer (Figure 3.2.1-4). Using a photomask and UV exposure, we produced a negative relief patterned master of the microwell array. Uncrosslinked photoresist was developed away (Figure 3.2.5-6). The exposed portion of the wafer (the bare silicon) was etched down to a desired well depth of 34 µm (61 loops), 50 µm (92 loops), or 100 µm (185 loops) using the Deep Silicon Etcher (Figure 3.2.7). Note: Each loop etches ~0.5 µm deep. The etched wafer was then placed in the hot strip bath for 1 hour followed by a 10 minute clean strip and 10 minute rinse to

produce the final silicon wafer master (Figure 3.2.8). The well dimensions were then directly measured for variations in shape and volume. Using a profilometer, we found the variation in well height to be <2% and the variation in the lateral well dimensions to be <2% as well.

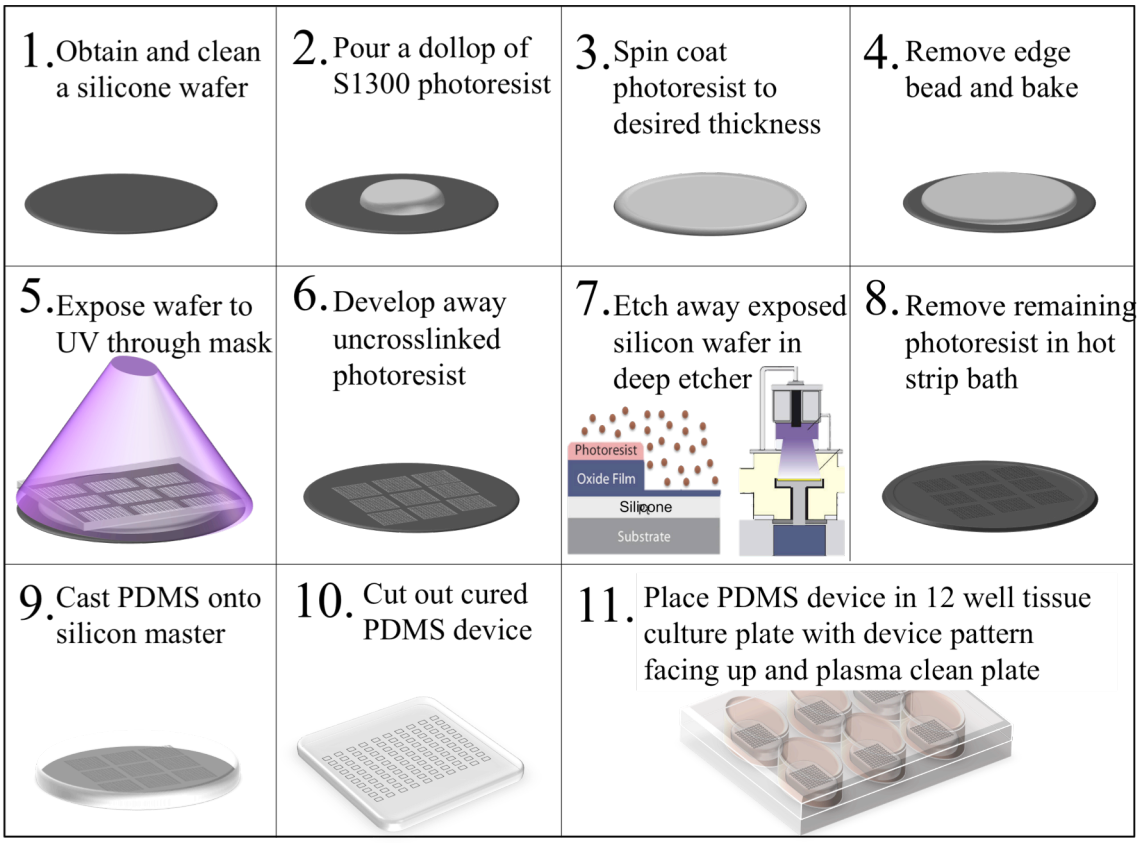

Figure 3.2 Microwell array device fabrication process.

3.1c Fabrication of the PDMS Stamp

Using replica molding techniques, PDMS was cured onto the etched silicon wafer and the pattern of interest was cut out (Figure 3.2.9-3.2.10). Steps 8-10 of Figure 3.2 illustrate the device fabrication from the master. Prior to casting the PDMS, the silicone masters were salinized using 20 µL of Dodecyl Triethoxysilane in a vacuum for 24 hours to facilitate removal of PDMS in subsequent steps. PDMS was then cast onto the master, cured for 1 hour at 60 °C and peeled

away. Individual devices were biopsy punched using a 12 mm diameter punch. Each device was placed on a 12-well cell culture multi-well plate (Figure 3.2.11).

3.2 Device as a suitable cell culture platform

3.2a Sterilization and Hydrophilicity treatment of PDMS

We treated each PDMS microwell array in an oxygen plasma vacuum desiccator for 3 minutes at pressure near 350-450 mTorr. Following plasma treatment, the devices were immediately immersed in a solution of 1% wt/vol BSA (bovine serum albumin) for 1 hour at 25°C and then rinsed with sterile PBS (phosphate buffered saline) in order to increase hydrophilicity and to minimize adhesion of cells to the wells.

3.2b Loading arrays of microwells

To determine the optimal cell seeding density, dilutions of cells were created from a cell suspension. Cell loading parameters were varied according to drop volume (60 or 30 μL) and total cell count (1600, 1800, 2000) to give 5 cell concentrations **(***e.g.* to increase the likelihood of having no more than one cell per microwell, a suspension of cells was diluted to $6x10^4$ cells/mL in serum-containing media and a 30 μL drop was pipetted onto the surface of the microwell array as shown in Figure 3.3.A-C). The cells were allowed to settle for 40 minutes. Media was carefully added to the well in order to completely submerge the device (Figure 3.3.D). Cells from randomly selected viewing fields were imaged using a 10x lens (Figure 3.3.E). The 'percentage of wells filled' and the 'average number of cells per well' were determined by counting the number of cells and averaging data collected from multiple microwell arrays (Figure 3.3.F).

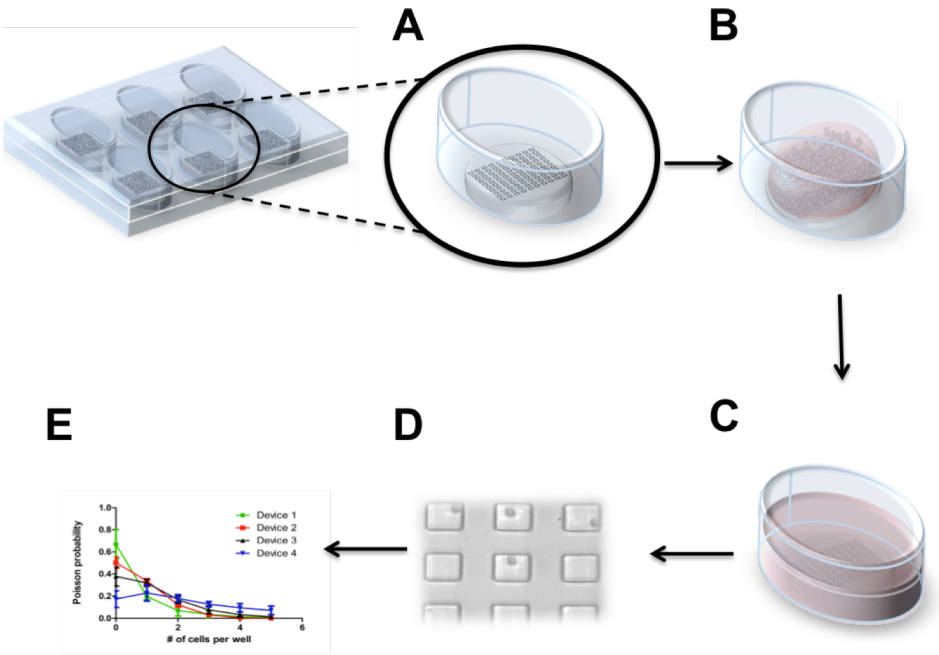

Figure 3.3 Diagram of seeding cells onto microwell array devices. The sterile 12 well tissue culture plate containing (A) the device is seeded with a drop of media containing cells (B) and allowed to settle for 40 minutes. Followed by the settling time, (C) the device is completely immersed in fresh media. Once the steps have been completed for all 12 wells containing devices, (E) the microwell arrays are imaged and (F) information on the devices obtained and quantified.

3.2c Characterization of cells

We examined viability and proliferation of cells in the microwells over the course of 96 hours using brightfield and fluorescence microscopy. Staining with 4',6-diamidino-2-phenylindole (DAPI) helped to automate the process. DAPI is a fluorescent stain that binds to A and T regions in the DNA strand, a strong candidate for fluorescence microscopy since DAPI can pass through even an intact cell membrane [66]. A primary antibody for CD38 (Abcam Anti-CD38 Rb pAb) was used with a secondary antibody (Goat anti-rabbit AlexaFluor®488). Brightfield images were taken every 24 hours for morphology and cell count monitoring for a total of 96 hours.

Critical step: Fluorescence imaging was performed without removing the microwell arrays from the culture device. Steps were performed by applying reagents to the media reservoir containing the microwell device and imaging through the base of device and well plate.

To fix the cells at experimental endpoints, media in the reservoir (or well plates) was replaced with 3.7% (wt/vol) formaldehyde in PBS, and the device was incubated at room temperature for 30 minutes. To remove the formaldehyde, three, 5 minute washes with PBS were performed. To block against non-specific binding and to permeablize the cell membranes for immunocytochemistry, wells were incubated in PBS with 3% BSA and 1% Triton-X for 1 hour. Another set of three, 5 minute washes with PBS was performed. Next, arrays were incubated with rabbit polyclonal primary antibody against CD38 (Abcam Anti-CD38 Rb pAb) in PBS (1:50 ratio) with supplemental 1 % BSA overnight at 4°C. Following three, 5 minute washes with PBS the wells were incubated in a dark room with secondary antibody (Goat anti-rabbit AlexaFluor®488) in 1:50 ratio in PBS with supplemental 1% BSA as well as DAPI in a 1:1000 ratio, for 1 hour at room temperature. A final set of three, 5 minute washes with PBS were performed.

Critical Step: Procedures with secondary antibodies and DAPI were performed in the dark. Visible light degrades the fluorophores that are conjugated to the antibodies and will prevent successful fluorescence imaging (however it is a *much* weaker degradation than that of the confocal laser). The culture devices were wrapped in aluminum foil during incubation and at all times afterwards to prevent exposure to light.

CHAPTER 4

RESULTS AND DISCUSSION

4.1 Device Design and Optimization

A large focus of this project was to fabricate a microwell array platform that could be readily replicated using soft lithography techniques and to establish a protocol for seeding and imaging cells in these devices. Our goal was to maximize single-cell wells in order to investigate differences in cell behavior (e.g. proliferation and differentiation) within a heterogeneous cell population (e.g. HL60 cells).

Initially, we explored four device designs that varied in well diameter and spacing (Table 4.1), as well as three different etch depths (30 μm, 50 μm, and 100 μm). Cells were seeded in each device and imaged at random locations following a forty-minute settling time. Additional images were taken at various intermediate time points up to 96 hours. The number of cells per well was counted. At least 10-12 replicates of each device were used and at least 245 wells in each replicate were tabulated.

Table 4.1 Well diameter and spacing between wells for each of 4 devices.

Device	**1**	**2**	**3**	**4**
Well Diameter (μm)	50	50	100	100
Well Spacing (μm)	50	50	100	300

4.1a Well Depth

Well depth was found to be an important design criterion for compatibility with live-cell imaging. Image clarity was compromised in the 100 μm deep wells due to an insufficient working distance of our microscope objective, rendering these devices unusable. An additional problem of "cell stacking" was also exacerbated in deeper wells, since multiple HL60 cells (10 μm average diameter) can fit vertically. The concern with wells shallower than 25 μm is the increased likelihood of cells being dislodged during a wash step or during transportation prior to imaging.

Part of our cell analysis requires we look for expression of the surface marker CD38 to determine whether or not HL60 cells have differentiated. The ability to perform immunohistochemical studies in the device is important not only for this pilot study, but for any future application of the device. Immunohistochemistry involved numerous wash steps, so we tested three well depths of 30 μm, 50 μm, and 100 μm to determine the loss of cells over the course of the protocol (Figure 4.1). Sample devices post 3 consecutive fix and wash steps are shown for each depth (Figure 4.2).

We found the optimal well depth (Figure 4.1) for our purposes to be 50 μm which retained 84% of the original cells after washes; whereas, the wells of 30 μm depth only retained 62% of the original cells. In the 50 μm depth, we determined that wells containing over 5-8 cells were typically dislodged, while wells containing 2-4 cells stayed in place. This was in large part due to the non-adherent property of HL60 cells, which remain in suspension. Depending on the cell type used, especially the adherent nature of the cells, shallower wells may be optimal.

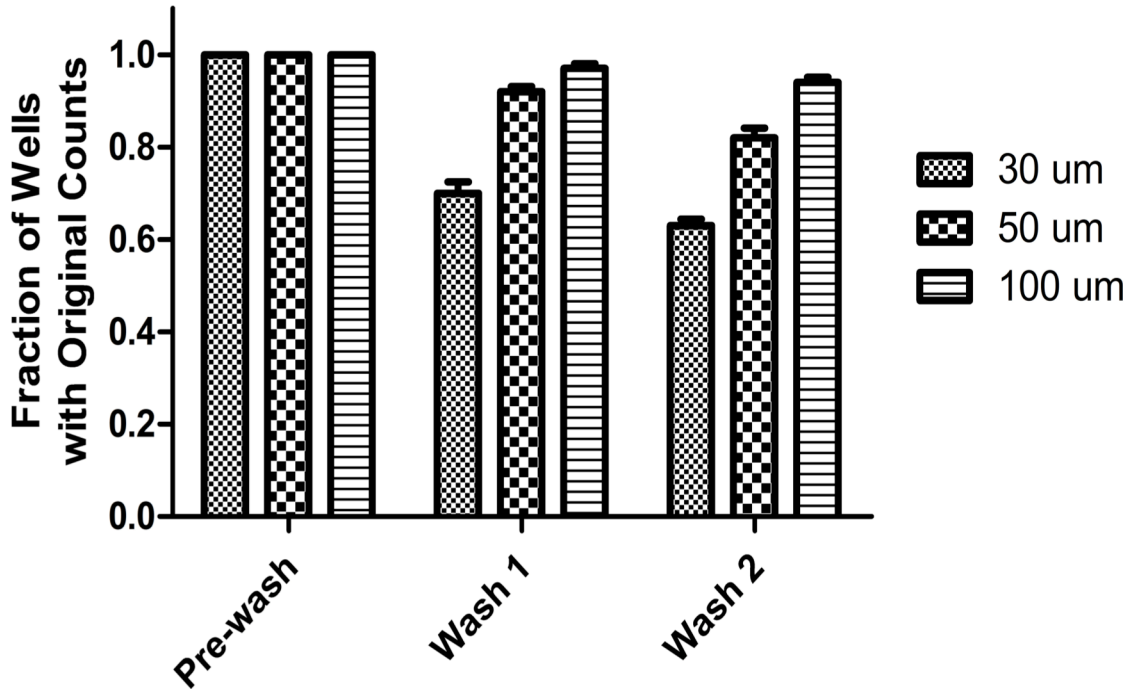

Figure 4.1 Cell retention post wash steps. The percentage of wells retaining their original cell from wash 1 to wash 2 are plotted for 100 µm, 50 µm, and 30 µm deep wells.

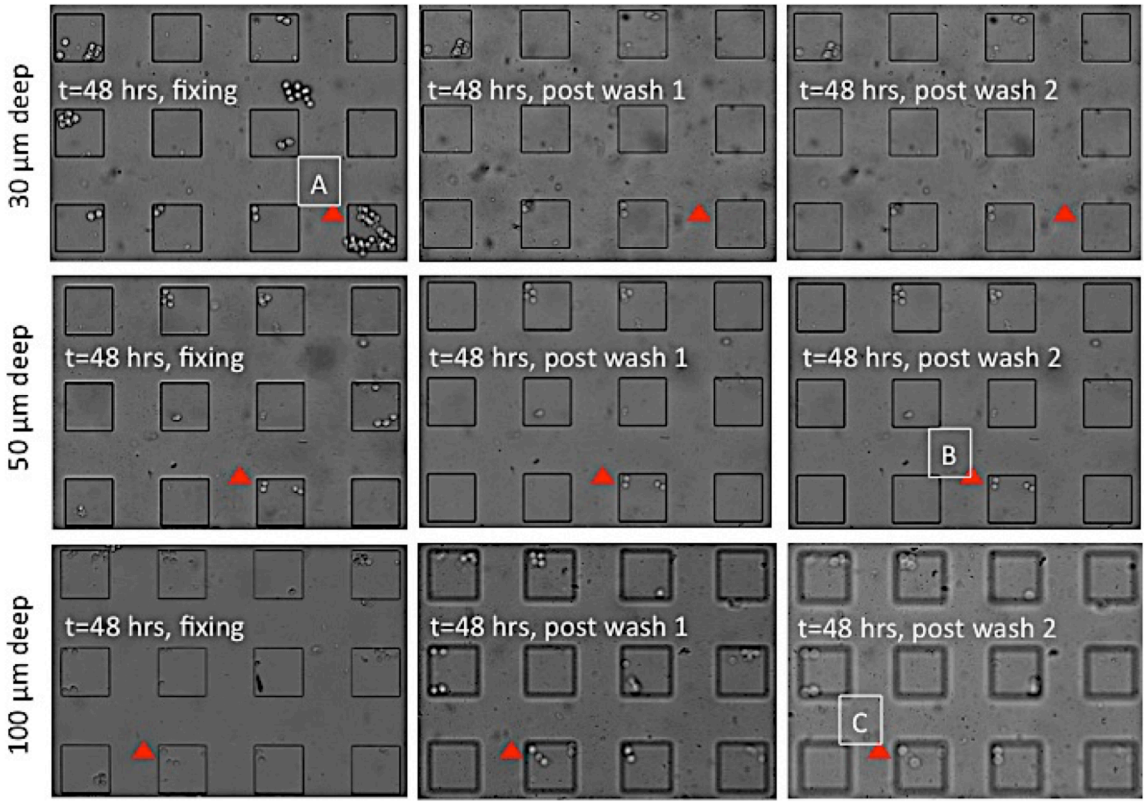

Figure 4.2 Well depth image quality. Fixing and staining followed by two wash steps were performed on each of the three devices 30 µm, 50 µm, and 100 µm depths imaged. A cluster of cells (A) in the 30 µm deep wells are dislodged after the initial wash step. After consecutive washes, cells (B) remain in the 50 µm well. Cells are visible in the 100 µm, but image quality is very poor.

4.1b Well Shape

Initially, we used a square slab exterior device design (Figure 4.3.A); however, with this device shape, the media droplet did not retain its spherical shape and spilled over the edges. This created fluctuations in seeding density and poor reproducibility. To overcome this, we used a circular 12 mm biopsy punch to cut out the devices. The droplet maintains a circular shape to distribute surface tension on all parts of the droplet equally (Figure 4.3.B) thereby achieving the lowest energy state. When it encounters the straight edge of the square, it creates a flat boundary, and the required surface tension is higher at the square corners (Figure 4.3.A). In conclusion, the circular device shape proved to be better suited for droplet stability, thereby minimizing variability in cell loading and controlling the surface area of the device exposed between replicate devices.

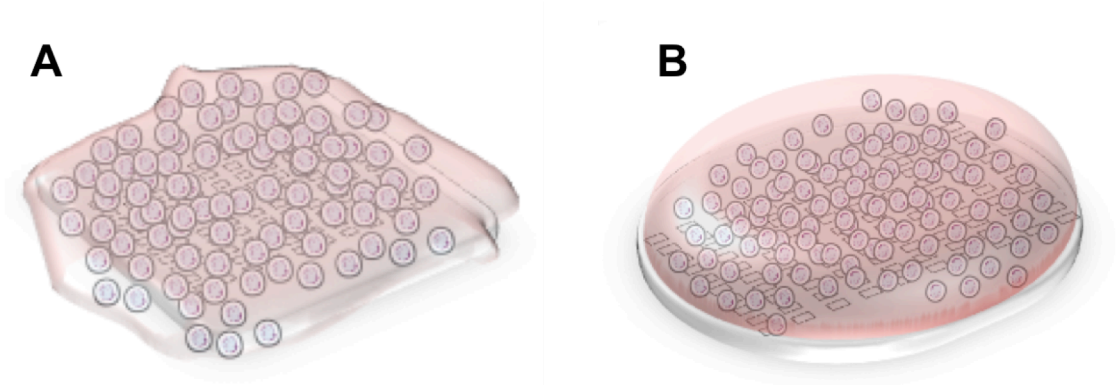

Figure 4.3 Illustrations of two different device shapes (A) square and (B) circular were studied. The square device (A) did not retain liquid droplets on the surface, whereas the circular device (B) was able to retain the structure of the liquid droplet for the duration of the 40 minute settling time of cells onto the device.

4.1c Well Diameter and Spacing

In determining the optimal device parameters for well dimensions and spacing between wells in the device (Table 4.1), we sought to 1) maximize the number of wells with a single cell and 2) minimize the number of empty wells.

Cells in a given microwell array device were manually counted in five representative regions, which included the corners and the center wells and spanned 240 representative wells out of 1600. We seeded 12 devices per condition (48 in total). Cell seeding distributions for each of the four devices are shown plotted in Figure 4.4. The probability of a cell settling within a well is independent of previous events and thus the likelihood of an event occurring can be described using a Poisson distribution. Poisson statistics were performed and the resulting Poisson distribution was compared to the calculated distribution.

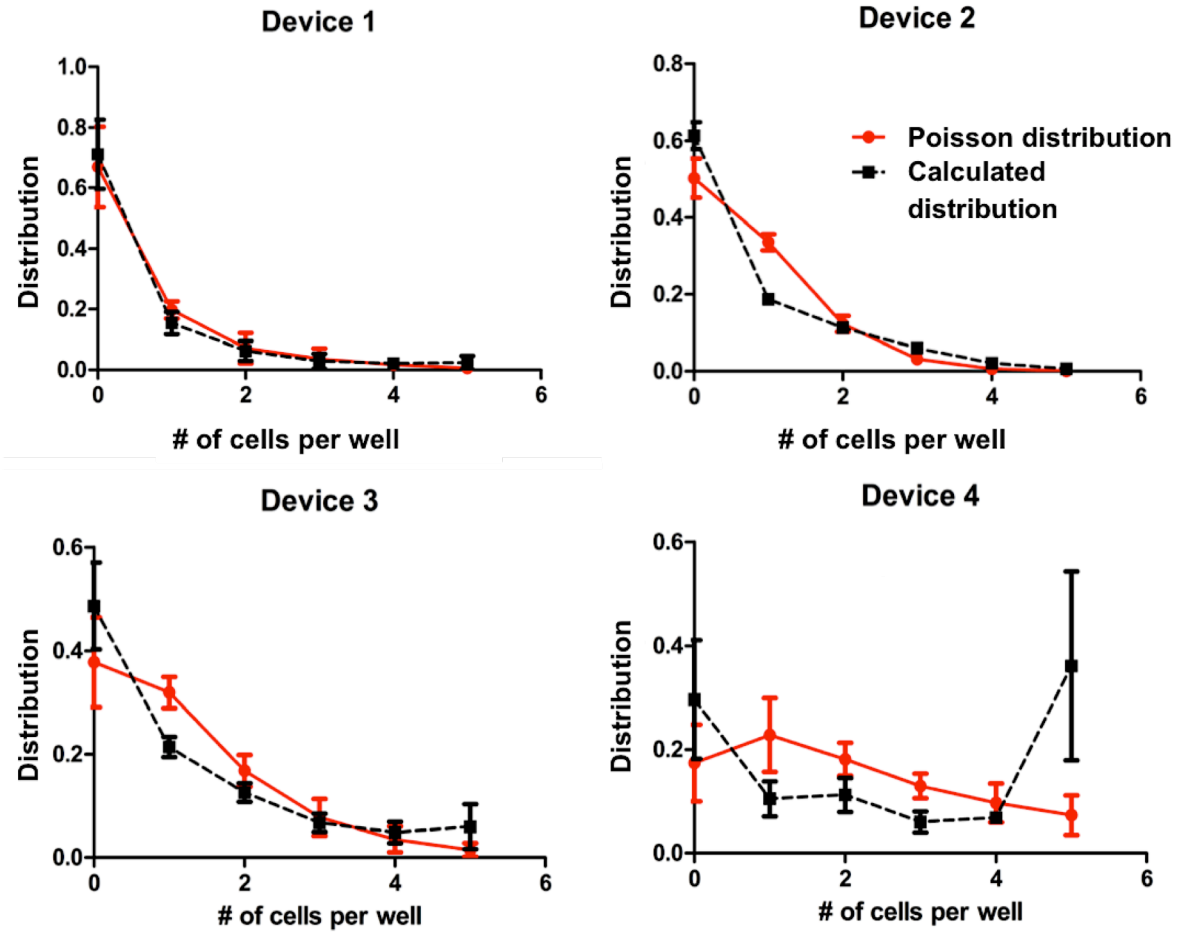

Figure 4.4 Poisson distributions for devices. Poisson statistics were performed on all 4 device types and plotted with their respective calculated number of cells per well distributions. The four device parameters are device1 (50 µm x 50 µm x 50 µm separated by 50 µm), device 2 (50 µm x 50 µm x 50 µm separated by 150µm), device 3 (100 µm x 100µm x 50 µm separated by 100 µm), device 4 (100 µm x 100 µm x 50 µm separated by 200 µm).

According to Figure 4.4, three of the four devices did not match their respective Poisson curves leading us to investigate what could affect the random nature of cell settling. Knowing that a cell is just 10 μm in diameter, we concluded random pattern was dependent on how easy it was for cells to settle onto the margins between wells. Device 1, which showed Poissonian distribution, had the smallest separation (50 μm separation) and would pose a significant challenge to cells trying to settle on the median versus the other devices (100 μm, 150 μm, and 300 μm separation). However, from the Device 1 distribution, we see that in fact Poisson statistics do accurately model the gravitational driven flow of cells into wells which corroborates what has been published by other groups using similar platforms [35, 36, 39].

As our main objective was to generate single cell wells, we performed an analysis similar to a Receiver Operating Characteristics (ROC) curve. A ROC curve compares the likelihood of correctly characterizing both positive and negative outcomes. The traditional use of a ROC curve is as a predictive tool, especially in epidemiology. However, we used it as a performance metric to determine the optimal device parameters for our study as is often done in machine learning. We defined 'sensitivity' as the percentage of wells with single cells (referred to in ROC statistics as the true positive rate). Specificity is typically defined as the true negative rate, or the ratio of true negative to sum of true negative and false positives. Because we have a non-binary output, we modified the 'specificity' value to fit our optimization criteria. On closer examination, the denominator in specificity is the sum of all actual negative cases, which in this case can be defined as all non-single cell wells. This metric allows us to minimize empty wells at the expense of having wells with more than one cell. In this way, we define our 'true negative' as

empty wells. This, specificity is defined as the ratio of empty wells to the sum of non-single cell wells, or shown in equation form:

$$\textit{Specificity} = \frac{\textit{True Negative}}{\textit{True Negaitve + False Positive}} = \frac{\textit{Wells with zero cells}}{\textit{Non-single cell wells}}$$

In this way, we generate a pseudo-binary outcome with single cell wells as the true positive, and empty wells as the true negative. This was chosen as the specificity based on the reasoning that non-empty wells could still yield data. In the future, these multi-cell wells could be used for other scenarios describing the effect of cell-cell contact on differentiation or metastasis compared to single cell studies, elucidating further mechanistic insight. The ROC curve indicates that Device 3 (100 µm x 100 µm x 50 µm separated by 100 µm) is closest to the ideal.

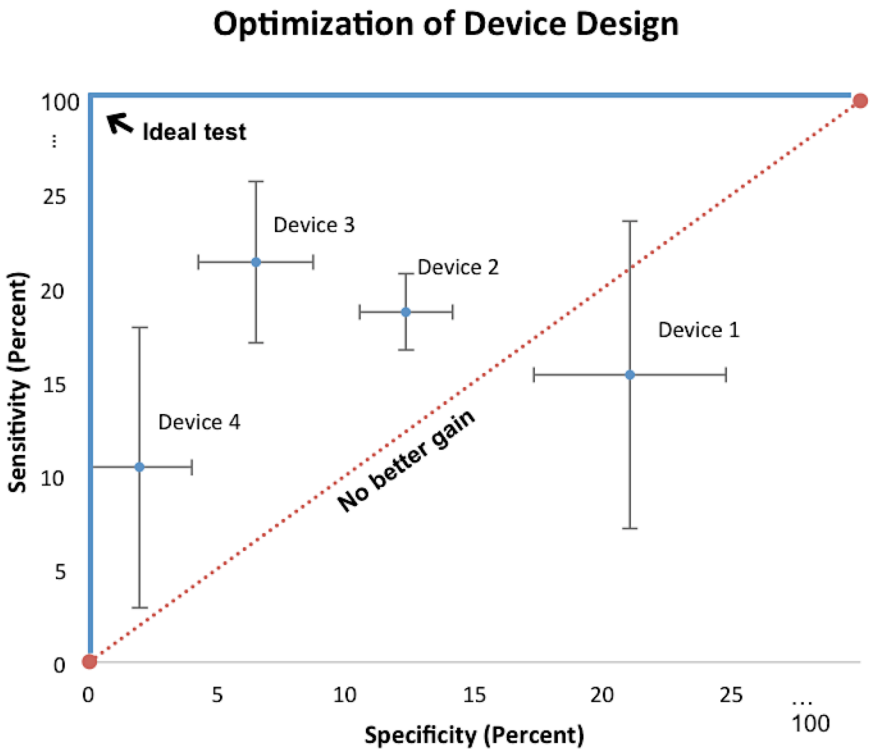

Figure 4.5 Optimization of device. We performed modified receiver operating curve statistics to determine optimal device for our study. Plotted above are the ideal condition and the no predictive value line along with the results for each device. Device 3 (100 µm x 100 µm x 50 µm separated by 100 µm), is the furthest away from the "no better gain" line.

4.1d Seeding Density

Having optimized the device parameters, we began working on seeding density to ensure reproducibility as well as maximize single cell wells. We found that multiple seeding densities and volumes produced similar probability distributions making the final selection somewhat arbitrary. However, with the other parameters set, this can easily be modified to fit the cell type and desired experimental outcome. We determined from our analysis (Figure 4.6) the optimal seeding density for the device to be 1800 cells/30 µL. Although this seeding density also matched the distribution of the 2000 cells/60 µL seeding, we chose the concentration that required less cells for future studies in which we are working with rare cells as well as smaller volumes of reagents that can cost on the order of hundreds of dollars for small volumes.

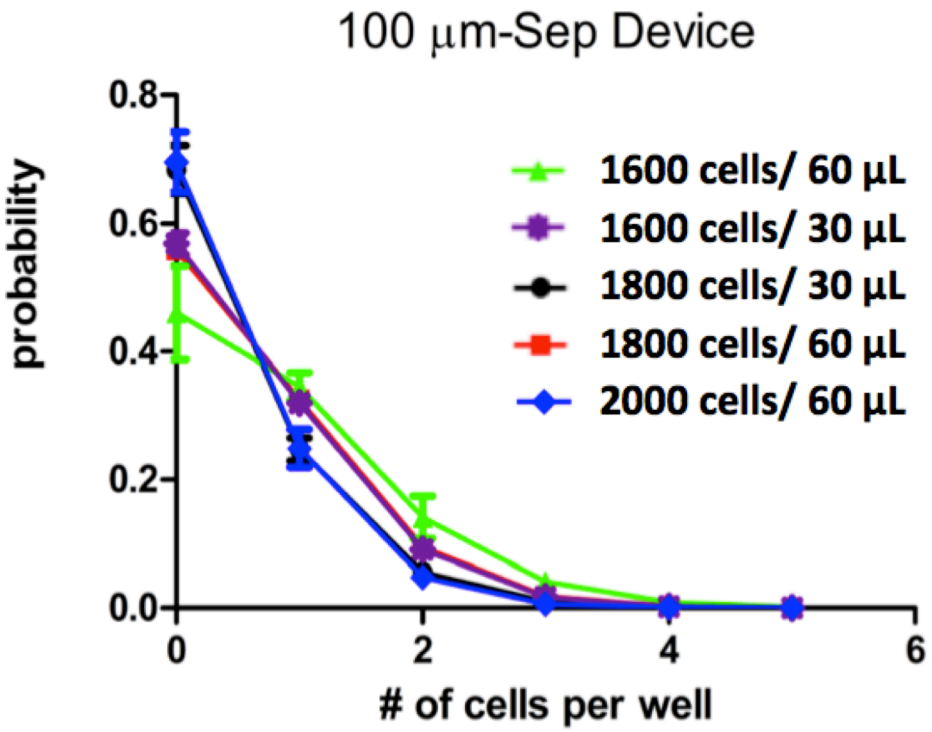

Figure 4.6 Poisson distributions for seeding concentration. There is considerable overlap between different concentrations making it difficult to determine the true optimal conditions. However, the seeding condition chosen was 1800 cells/ 30 µL.

4.2 Proof of Principle Experiments

4.2a Live Cell Imaging Using HL60

To prove that the device could be used as a live cell imaging platform we showed that cells were viable for up to 96 hours (the length of time of a differentiation experiment is at least 36 to 48 hours) in our microwell array (Figure 4.7.D).

4.2b HL60 Growth Curves

The stochastic nature of cells is illustrated by a cell proliferation study. We looked at viability of individual cells in the device over the course of 96 hours, plotting only to 48 hour time points for illustrative clarity (Figure 4.7.A). For a cell line with an expected doubling time of 36-48 hours [18], when broken down to a single cell level, we see a variation of 0-10 cells per well over this same time frame (Figure 4.7.A). This variation is explained in the illustration to the right of the graph, indicating that at 24 hours a cell can undergo death, division, or no change (Figure 4.6.B). We determined the average doubling time of HL60 to be 24 hours using a small sample size of 24 cells compared to typical bulk cell conditions of cell counts anywhere between 0.2-2 x 10^6 cells/mL in a typical 10 mL flask. The average growth of the cells in the device was determined to be 24 hours (Figure 4.7.C), and the standard deviation (±1.23 cells/well) of cell growth over the course of 48 hours alone clearly indicates the heterogeneity seen within even a homogenous cell population, which is typically masked by average bulk-cell growth behavior.

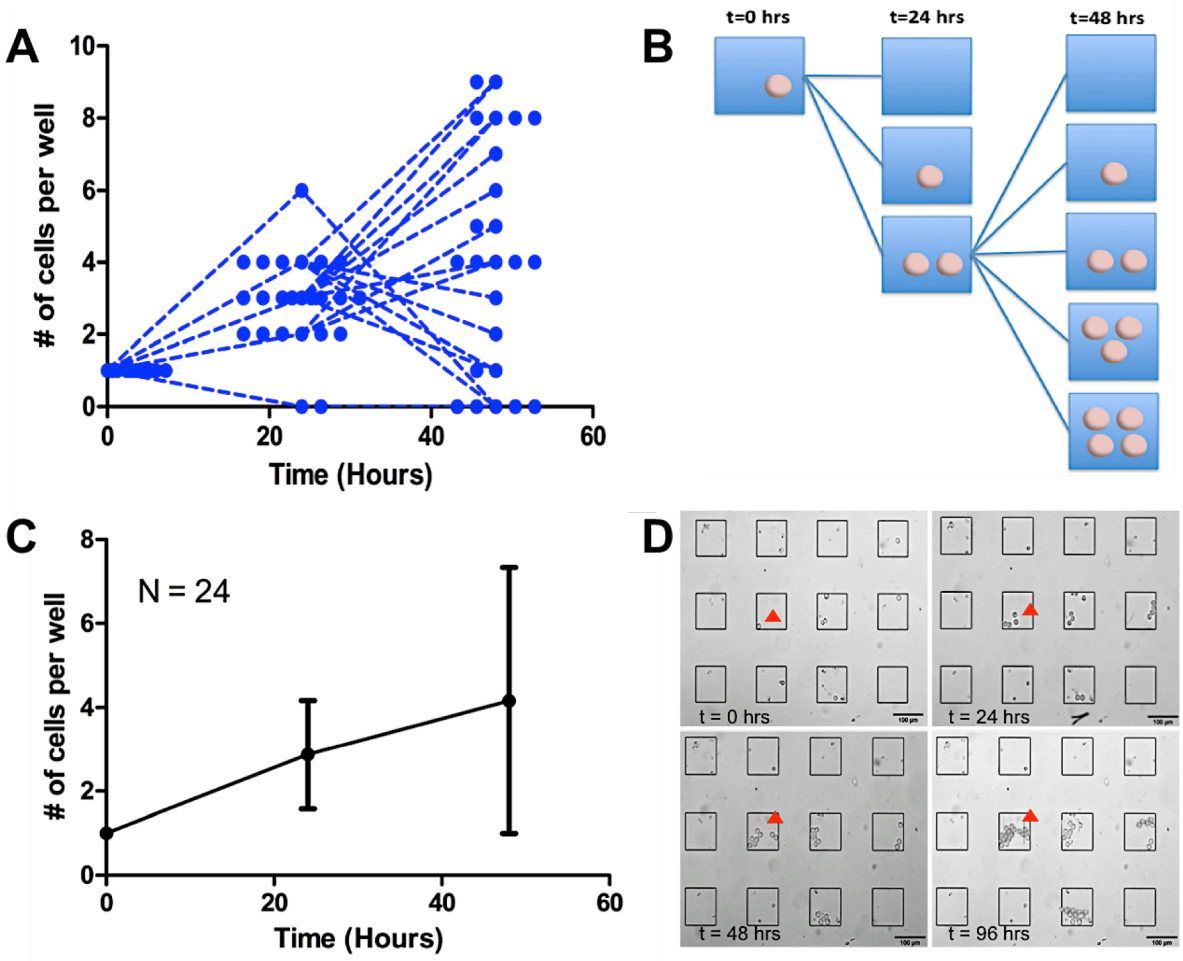

Figure 4.7 Growth curves of individual cells. Growth of individual cells (A) over the course of 48 hours and their averages (C). An illustration (B) of the reasons for the different scenarios a given cell can undergo over just 48 hours providing some insight into the level of variation found in (D). Live cell images of wells taken every 24 hours for a total of 96 hours indicates the viability of cells in the well for the duration of a full experiment.

4.2c Induction of Granulocytic Differentiation

To characterize heterogeneity within a cell population and to understand some of the complexity of cell behavior in response to a stimulus, we studied the differentiation of HL60 by all-trans retinoic acid (ATRA), a specific and potent inducer of HL60 to granulocyte-like maturation [48]. While we were unable to determine the rate of differentiation, we were successful in identifying differentiated cells based on expression of CD38 surface markers. We used secondary immunofluorescence—multiple secondary antibodies bind to a single primary antibody – to

amplify signal output. The unlabeled primary antibody (anti-CD38 Rabbit monoclonal antibody) specifically binds to the target molecule CD38, while the secondary antibody, which carries the fluorophore (goat anti-rabbit Alexa flour 488), recognizes the primary antibody and binds to it.

Since CD38 detection at the surface begins around 36 hours post treatment with ATRA, we fixed cells at 48 hours and stained with an anti-CD38 antibody (Figure 4.10, 4.11). The 24 hour time point was used as a comparison.

As expected, neither ATRA treated (Figure 4.9) nor untreated (Figure 4.8) cells express CD38 at the surface after 24 hours. Cells were imaged using brightfield microscopy. From the live cell images obtained, some cells proliferated while others stayed the same or died within the 24 hour time period. In this set of experiments, cells were fixed and stained with DAPI and CD38 primary antibody followed by a secondary antibody containing flourophore. The DAPI stains the nuclei of all the cells (Figure 4.8.A, Figure 4.9.A) while CD38 is only expressed in treated and differentiated HL60 cells. At 24 hours post treatment with ATRA, there is no visible expression of the marker (Figure 4.8.B, Figure 4.9.B).

Live cell imaging was also performed on both untreated cells (Figure 4.10) and cells treated with ATRA (Figure 4.11). The cells were fixed and stained at the 48 hour time point. In both devices, cells stained with DAPI showed a strong signal (Figure 4.10.A, Figure 4.11.A). The non-treated device did not visibly express CD38 (Figure 4.10.B). However, devices containing treated cells displayed fluorescence as expected (Figure 4.11.C).

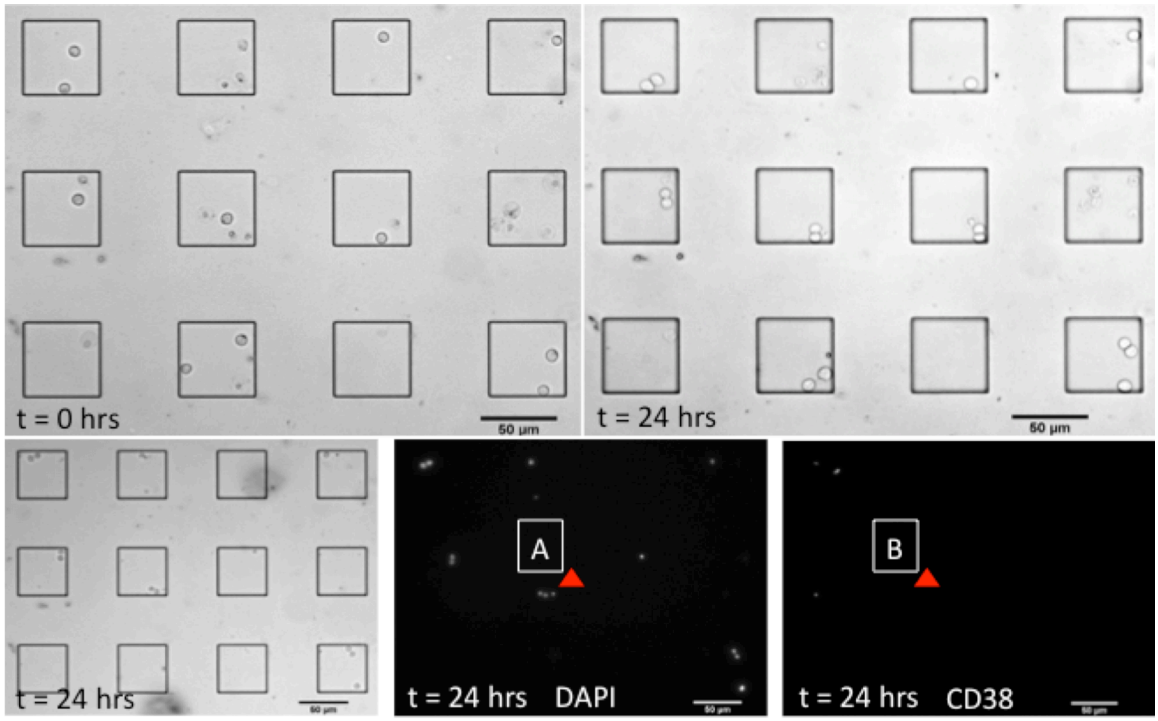

Figure 4.8 Cells at 24 hours with No ATRA. Live cell (top row) and fixed cell (bottom row) images of HL60 cells after 24 hours. DAPI was used to stain the (A) nuclei of cells and a green fluorophore used as a secondary antibody for binding to CD38 primary antibody. There is no visible (B) CD38 expression.

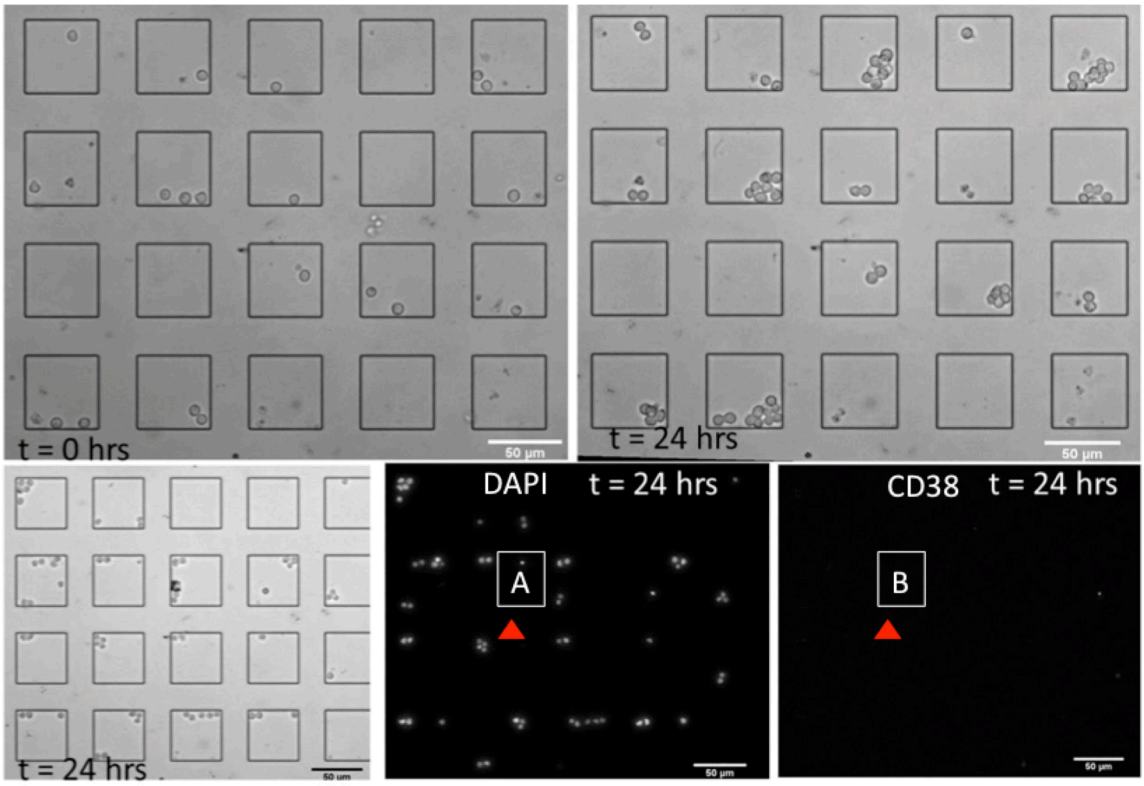

Figure 4.9 Cells at 24 hours with ATRA treatment. Live cell (top row) and fixed cell (bottom row) images of cells after 24 hours post treatment with ATRA. Cell nuclei are illuminated with (A) DAPI; however, there is no visible (B) CD38 expression.

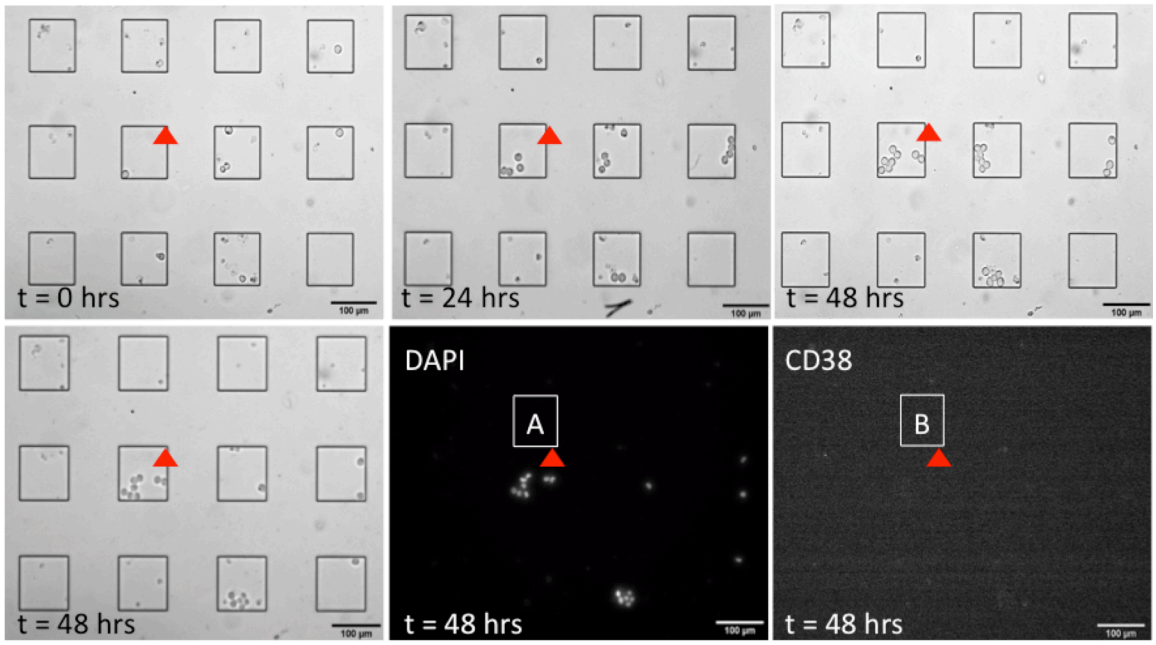

Figure 4.10 Cells at 48 hours with no ATRA. Live cell (top row) and fixed cell (bottom row) images of HL60 cells after 48 hours of incubation. DAPI staining is visible in wells corresponding to the brightfield image in which cells are visible. There is no visible CD38 expression as expected.

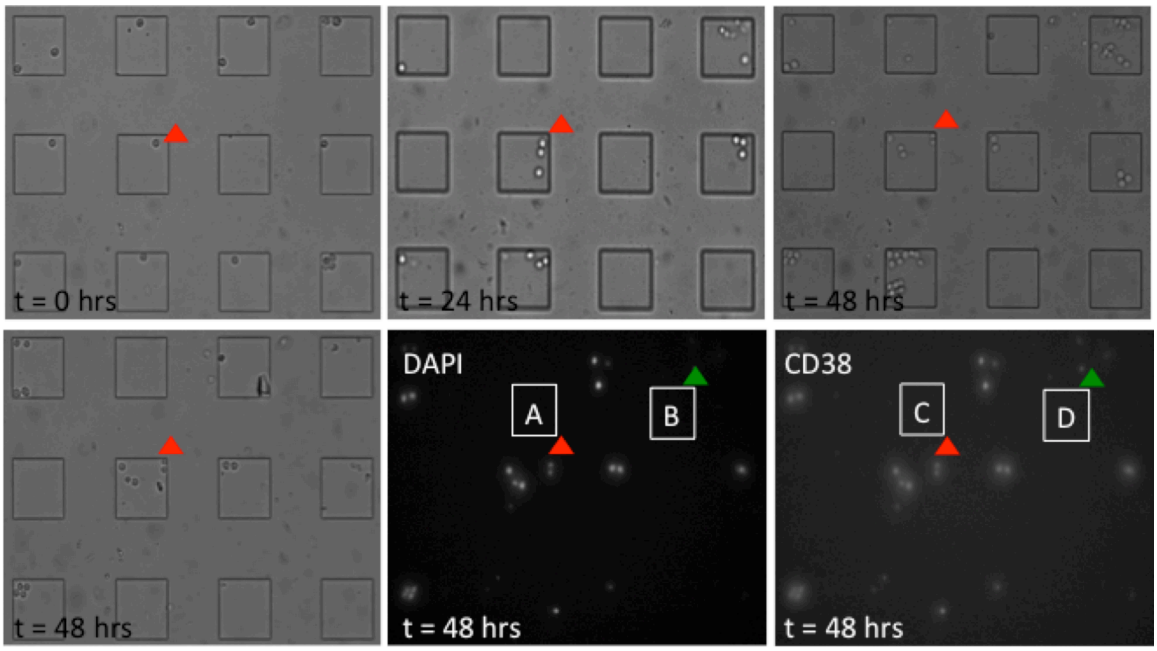

Figure 4.11 Cells at 48 hours with ATRA treatment. Live cell (top row) and fixed cell (bottom row) images of cells 48 hours post treatment with ATRA. There is visible CD38 expression (C) corresponding to areas where we see visible DAPI staining (A) as expected. We also see some non-specific binding of antibody to cell debris (D) that does not correspond to a whole cell (B) likely due in part to use of a polyclonal secondary antibody.

4.2d Adherent Cell Lines and Broader Applications

We showed that our device is not cell type specific; the device can be applied to any cell lineage of interest. HL60 is a non-adherent robust cell line, but we show that our device also proves to be a useful platform for a more sensitive and less robust line of adherent type, like primary human umbilical vein endothelial cells (HUVECs). Again, we determined that, after just 20 minutes, the cell line displayed growth and adherence to the device. Furthermore, hourly imaging showed the cell line's viability over the course of 48 hours (Figure 4.12) (only shown to the 24 hour time point). A red arrow indicates an individual cell that is tracked across the different frames, illustrating the motility of a cell within the microwell.

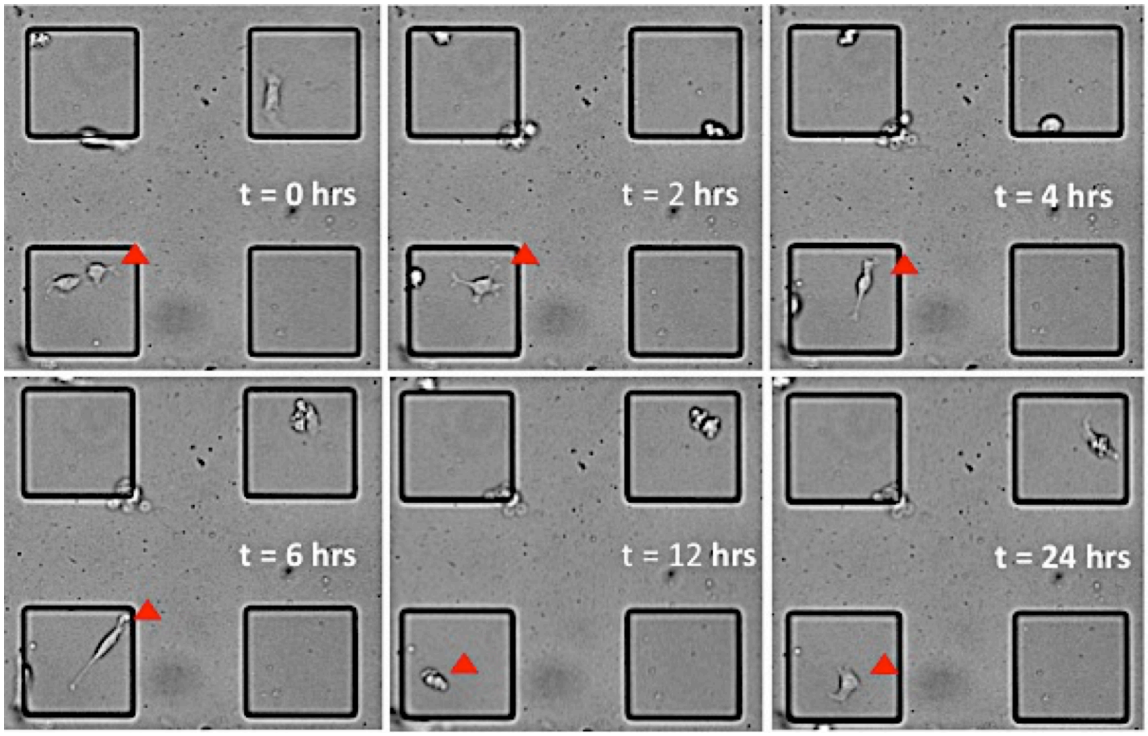

Figure 4.12 Device application is not cell type specific. HUVEC cells imaged in the microwell array platform adhered within the 40 minute settling time on the device (t=0 hours), and were imaged every hour for 48 hours (only shown to 24 hours). The red arrow provides a marker for ease of following the same cell across corresponding frames.

CHAPTER 5

PERSPECTIVES/FUTURE DIRECTIONS

Bulk-scale measurements made on a heterogeneous population of cells report only average values for the population and are not capable of determining the contributions of individual cells. However, properties such as viability, protein concentration, or possession of a mutant allele, are discrete and intrinsic states of each individual cell. Methods capable of analyzing these properties at the level of the individual cell enable a more complete understanding of phenomena that are inaccessible to researchers using population-scale approaches.

5.1 Improve automated cell counting

Attempts at generating automated cell counting were unsuccessful due to low image resolution. The primary difficulty was in resolving intact cells versus cellular debris. Another issue that was noted was the ability of ImageJ to appropriately detect cells that were clumped together or were located along the well wall. With improved lighting and resolution, ImageJ should become a viable tool for automation. We are confident that the device depth is shallow enough to allow for adequate imaging and that the automation of imaging with the microscope caused the images to be out of focus due to device shifting or incorrect execution of the automation. This could be resolved by implementing a more accurate software or installing a well plate stage mount to reduce device shift during imaging. Measures such as staining the cells to increase contrast or implementing further image processing steps may improve the accuracy of the program. Current efforts are focused on writing a custom Matlab code to quantify cell count in the devices. However, we face many of the same issues in Matlab that ImageJ could not resolve.

5.2 Paracrine signaling within HL60 cells

Based on our current approach of examining surface marker expression, the most information obtained from a given study is correlative data. Future studies will incorporate inhibition or upregulation of components in the ERK/MAPK cascade, which can provide insight into the signaling networks involved in HL60 differentiation [52]. In connection with the HL60 differentiation within a microwell array, conditioned media studies can be performed to determine whether or not cells are truly isolated in their wells. We should be able to show that single cells do or do not differentiate and whether or not there is in fact no communication between the wells. Currently work is underway to transfect HL60 cells to create reporter cell lines to indicate differentiation when induced. Our platform could allow for time-lapse studies to watch the process of differentiation live instead of the labor and time intensive process of completing immunohistochemistry at multiple time points. It is currently unclear whether or not both mother and daughter cells differentiate post treatment in the final division step prior to differentiation or if only the daughter (or mother) cell differentiates in the process [54, 63]. Through this induced reporter approach applied to cells within our microwell array, we can study this mechanism of differentiation.

5.3 CTCs and Geometrically Enhanced Differential Immunocapture (GEDI)

Current methods of determining CTC presence in the blood stream involve cellular capture assays that require multiple manipulations in which cells are mechanically damaged and physically lost [71]. Over the last decade, a highly automated immunoseparation and characterization system CellSearch has been developed and is currently the only FDA approved CTC collection device. The immune-separation component of this system is based on microscopic ferrous particles that remain in suspension and that have been coated with a

monoclonal antibody directed against EpCAM in order to bind presumably epithelial cells, *e.g.* CTCs [69]. However, this assay renders the CTCs collected from the sample useless for further use and interrogation studies. The only information obtained is CTC count. This information can aid in determining prognosis and maybe provide information on effect of current treatment approaches but does little in terms of helping address or tackle the issue of personalized medicine for improved cancer treatment.

The GEDI (geometrically enhanced differential immunocapture) device designed and tested by the Kirby group here at Cornell University resolves the issue of capturing the cells for further analysis post initial device assessment. The GEDI microdevice geometry selects out CTCs by maximizing streamline distortion and increasing collision frequency of the desired cells in order to bring them into contact with the immunocoated walls for capture [70]. Even with use of cellular preservative, CTC detection declines after storage for more than 96 hours. Currently, this technology limits use of archived specimens, necessitating prospective studies to enumerate and characterize cells. For example, assessment of the proliferative activity of circulating tumor cells may be important in understanding failure of cytotoxic chemotherapy regimens to eliminate disseminated cells in a substantial number of patients with breast cancer. A simple estimate to assess proliferative activity versus cell cycle arrest *in situ* is immunostaining for expression of the Ki-67 antigen, which is absent in the G0 and early G1 phases of the cell cycle [56, 67]. The GEDI device coupled with our microwell array design can aid in better characterizing CTCs to enhance capture and to improve cell output, but also, analysis of these CTCs in the context of our device may provide a non-invasive approach to assessment of prognosis and appropriate treatment for established cancers.

CHAPTER 6

SUMMARY

Bulk-scale measurements made on a heterogeneous population of cells report only average values for the population and are not capable of determining the contributions of individual cells. Methods capable of analyzing these properties at the level of the individual cell enable a more complete understanding of phenomena that are inaccessible to researchers using population-scale approaches. Cell heterogeneity is ultimately the reason for performing single cell level studies. How do we understand disease progression such as breast cancer? How can we knock down mean behavior in a cell line without potentially developing resistance in some cells? These are questions we continue to seek answers to. Not all cells are created equal, so by using microwell arrays as single cell platforms we can select for certain cells based on their response to a specific stimuli. By building devices to query populations of cells at a small group or single cell level, we can interrogate cell behavior one piece at a time which can provide insight into tumor development and signaling. This study explores and builds on the tools available for live cell single cell culture within a microwell array platform. We determined the optimal device parameters for single cell analysis of HL60 to consist of well dimensions 100 μm x 100 μm x 50 μm separated by 100 μm in an array on a disk shaped slab and an optimal seeding density of 1800 cells/ 30 μL. Future work intends to explore cell-cell interactions and perform analyses on rare cells, specifically circulating tumor cells, to inform patient diagnoses and treatment.

BIBLIOGRAPHY

1. Levsky JM, Singer RH. Gene expression and the myth of the average cell. *Trends in Cellular Biology*. 2003; 13:4–6.
2. El-Ali J, Sorger PK, Jensen KF. Cells on chips. *Nature.* 2006; 442:403–411.
3. Longo D, Hasty J. Dynamics of single-cell gene expression. *Molecular Systems Biology*. 2006; 2:64.
4. Gebhardt R. Metabolic zonation of the liver: regulation and implications for liver function. *Pharmacology Theory*. 1992; 53:275–354.
5. Rao CV, Wolf DM, Arkin AP. Control, exploitation and tolerance of intracellular noise. *Nature*. 2002; 420:231–237.
6. Raser JM, O'Shea EK. Noise in gene expression: origins, consequences, and control. *Science*. 2005; 309:2010–2013.
7. Elowitz MB, Levine AJ, Siggia ED, Swain PS. Stochastic gene expression in a single cell. *Science*. 2002; 297:1183–1186.
8. Di Carlo D, Lee LP. Dynamic single-cell analysis for quantitative biology. *Analytical Chemistry*. 2006; 78:7918–7925.
9. Rettig JR, Folch A. Large-scale single-cell trapping and imaging using microwell arrays. *Analytical Chemistry*. 2005; 77:5628–5634.
10. Cheung, K. J., Gabrielson, E., Werb, Z., & Ewald, A. J. (2013). Collective invasion in breast cancer requires a conserved basal epithelial program. *Cell*, *155*(7), 1639–1651.
11. Chin VI, Taupin P, Sanga S, Scheel J, Gage FH, Bhatia SN. Microfabricated platform for studying stem cell fates. *Biotechnology and Bioengineering*. 2004; 88:399–415.
12. Biran I, Walt DR. Optical imaging fiber-based single live cell arrays: a high-density cell assay platform. *Analytical Chemistry.* 2002; 74:3046–3054.
13. Maheswaran S and Haber DA: Circulating tumor cells: a window into cancer biology and metastasis. *Current Opinion in Genetics and Development* 20: 96-99, 2010.
14. Pantel K, Brakenhoff RH and Brandt B: Detection, clinical relevance and specific biological properties of disseminating tumour cells. *Nature Review Cancer* 8: 329-340, 2008.
15. Gallagher, B. A., Metzgar, R., Collins, S., Trujillo, J., & Ting, R. (1979). Characterization of the Continuous, Differentiating Myeloid Cell Line (HL60) From a Patient With Acute Promyelocytic Leukemia, *Blood. 54*(3).
16. Collins, S. J., Ruscetti, F. W., Gallagher, R. E. & Gallo, R. C. (1978) *Proceedings of National Academy of Sciences* USA 75,2458-2462. 15.
17. Collins, S. J., Bodner, A., Ting, R. & Gallo, R. C. (1980) *International Journal of Cancer* 25, 213-218.
18. Breitman I, Selonick S, Collins S: Induction of differentiation of the human promyelocytic leukemia cell line (HL60) by retinoic acid. *Proceedings of National Academy of Sciences* USA 77:2936, 1980
19. Newburger, P. E., Chovaniec, M. E., Joel, S., & Cohen, H. J. (1979). Functional Changes in human leukemic cell line HL-60 A Model for Myeloid Differentiation. *Journal of Cell Biology*, *82*(August).
20. Carey, S. P., Starchenko, A., McGregor, A. L., & Reinhart-King, C. a. (2013). Leading malignant cells initiate collective epithelial cell invasion in a three-dimensional heterotypic tumor spheroid model. *Clinical and Experimental Metastasis*, *30*, 615–630.
21. Souchier C, Brisson C, Batteux B, Robert-Nicoud M, Bryon PA. Data reproducibility in fluorescence image analysis. *Methods in Cell Science*. 2003; 25:195–200.
22. R Development Core Team. R: A Language and Environment for Statistical Computing. Vienna, Austria: R Foundation for Statistical Computing; 2008.
23. King KR, Wang S, Irimia D, Jayaraman A, Toner M, Yarmush ML. A high-throughput microfluidic real-time gene expression living cell array. *Lab on a Chip*. 2007; 7:77–85.
24. Revzin A, Sekine K, Sin A, Tompkins RG, Toner M. Development of a microfabricated cytometry platform for characterization and sorting of individual leukocytes. *Lab on a Chip*. 2005; 5:30–37.
25. Melamed, M. R. (2001). A brief history of flow cytometry and sorting. *Methods in Cell Biology*, *63*, 3–17.
26. Mandy, F. F., Bergeron, M., & Minkus, T. (1995). Principles of flow cytometry. *Transfusion Science*, *16*(4), 303–314.
27. Givan, a L. (2001). Principles of flow cytometry: an overview. *Methods in Cell Biology*, *63*, 19–50.

28. Salzman, H.M., Singham, S.B., Johnston, R.G. and Bohren, CF. (1990) Light scattering and cytometry. In: *Flow Cytometry and Sorting*, 2nd edn. (Eds. M.R. Melamed, T. Lindmo and M.L. Mendelsohn). Wiley, New York, pp. 81-107.
29. Julius MH, Masuda T, Herzenberg LA (1972). "Demonstration that antigen-binding cells are precursors of antibody-producing cells after purification with a fluorescence-activated cell sorter". *Proceedings of the National Academy of Sciences. U.S.A.* 69 (7): 1934–8.
30. Darzynkiewicz, Z., Bedner, E., Li, X., Gorczyca, W., & Melamed, M. R. (1999). Laser-scanning cytometry: A new instrumentation with many applications. *Experimental Cell Research*, *249*, 1–12.
31. Di Carlo D, Lee LP. Dynamic single cell analysis for quantitative biology. *Analytical Chemistry*. 2006; 78: 7918–7925.13.
32. Elowitz MB, Levine AJ, Siggia ED, Swain PS. Stochastic gene expression in a single cell. *Science*. 2002; 297:1183–1186.10.
33. Blake WJ, M KA, Cantor CR, Collins JJ. Noise in eukaryotic gene expression. *Nature* 2003; 422:633–637
34. Kane RS, Takayama S, Ostuni E, Ingber DE, Whitesides GM. Patterning proteins and cells using soft lithography. *Biomaterials* 1999; 20:2363–2376.17.
35. Moeller, H. C., Mian, M. K., Shrivastava, S., Chung, B. G., & Khademhosseini, A. (2008). A microwell array system for stem cell culture. *Biomaterials*, *29*, 752–763.
36. Molter, T. W., McQuaide, S. C., Suchorolski, M. T., Strovas, T. J., Burgess, L. W., Meldrum, D. R., & Lidstrom, M. E. (2009). A microwell array device capable of measuring single-cell oxygen consumption rates. *Sensors and Actuators, B: Chemical*, *135*(2), 678–686.
37. Deutsch, M., Deutsch, A., Shirihai, O., Hurevich, I., Afrimzon, E., Shafran, Y., & Zurgil, N. (2006). A novel miniature cell retainer for correlative high-content analysis of individual untethered non-adherent cells. *Lab on a Chip*, *6*, 995–1000.
38. Meek, C. C., & Pantano, P. (2001). Spatial confinement of avidin domains in microwell arrays. *Lab on a Chip*, *1*, 158–163.
39. Love, J. C., Ronan, J. L., Grotenbreg, G. M., van der Veen, A. G., & Ploegh, H. L. (2006). A microengraving method for rapid selection of single cells producing antigen-specific antibodies. *Nature Biotechnology*, *24*(6), 703–7.
40. Collins, S. J. and Gallagher, R. E. The HL-60 Promyelocytic Leukemia Cell Line: Proliferation, Differentiation, and Cellular Oncogene Expression. *The Journal of The American Society of Hematology*, *70*(5), 1233–1244.
41. H. Tanaka, E. Abe, C. Miyauri, T. Kuribayashi, K. Konno, Y. Nishii, T. Suda. 1,25-dihydroxycholecalciferol and a human myeloid leukaemia line (HL60); the presence of a cytosol receptor and induction of differentiation. Biochemical Journal, 204 (1982), p. 713.
42. Colston, M.J. Colston, A.H. Fieldstein, D. Feldman. 1,25-dihydroxyvitamin D_3 receptors in human epithelial cancer cell lines.Cancer Research, 42 (1982), p. 856.
43. R.J. Frampton, L.J. Suva, J.A. Eisman, D.M. Findlay, G.E. Moore, J.M. Moseley, T.J. Martin. Presence of 1,25-dihydroxyvitamin D_2 receptors in established human cancer cell lines in culture. *Cancer Research*, 42 (1982), p. 1116
44. A. Eisman, L.J. Suva, E. Sher, P.J. Pearce, J.W. Funder, T.J. Martin. Frequency of 1,25-dihydroxyvitamin D3receptors in human breast cancer. Cancer Research, 41 (1981), p. 5121
45. Collins, S. J., Gallo, R. C., & Gallagher, R. E. (1977). Continuous growth and differentiation of human myeloid leukaemic cells in suspension culture. *Nature*, *270*(24), 347–349.
46. McCarthy, D. M., San Miguel, J. F., Freake, H. C., Green, P. M., Zola, H., Catovsky, D., & Goldman, J. M. (1983). 1,25-dihydroxyvitamin D3 inhibits proliferation of human promyelocytic leukaemia (HL60) cells and induces monocyte-macrophage differentiation in HL60 and normal human bone marrow cells. *Leukemia Research*, *7*(1), 51–55.
47. Collins, S. J., Ruscetti, F. W., Gallagher, R. E. & Gallo, R. C. (1979) *Journal of Experimental Medicine*. 149, 969-974.
48. Yalcintepe, L., Albeniz, I., Adin-Cinar, S., Tiryaki, D., Bermek, E., Graeff, R. M., & Lee, H. C. (2005). Nuclear CD38 in retinoic acid-induced HL60 cells. *Experimental Cell Research*, *303*, 14–21.
49. Liu, Q., Kriksunov, I., Graeff, R., Munshi, C., Hon, C. L., & Hao, Q. (2005). Crystal structure of human CD38 extracellular domain. *Structure*, *13*, 1331–1339.
50. Visvader, J. E., & Lindeman, G. J. (2008). Cancer stem cells in solid tumours : accumulating evidence and unresolved questions. Nature Review Cancer. *8*, 755–768.

51. Kelly, P. N., Dakic, A., Adams, J. M., Nutt, S. L., & Strasser, A. (2007). Tumor Growth Need Not Be Driven. *Science*, 100.
52. Quintana, E., Shackleton, M., Sabel, M. S., Fullen, D. R., Johnson, T. M., & Morrison, S. J. (2008). Efficient tumour formation by single human melanoma cells. *Nature*, *456*(December).
53. Condeelis, J., Segall, J. E., & Einstein, A. (2003). ntravital imaging of cell movement in tumors. *Nature Reviews Cancer*, *3*(December), 921–930.
54. Karnoub, A. E., Dash, A. B., Vo, A. P., Sullivan, A., Brooks, M. W., Bell, G. W., … Weinberg, R. A. (2007). Mesenchymal stem cells within tumour stroma promote breast cancer metastasis, *449*(October).
55. Brabletz, T., Jung, A., Spaderna, S., Hlubek, F., & Kirchner, T. (2005). Migrating cancer stem cells — an integrated concept of malignant tumour progression, *5*(September), 744–749.
56. Pantel K, Alix-Panabieres C and Riethdorf S: Cancer micrometastases. *Nature Review Clinical Oncology*. 6: 339-351, 2009.
57. Kalluri, R., & Weinberg, R. A. (2009). Review series: The basics of epithelial-mesenchymal transition, *119*(6).
58. Ashworth A: A case of cancer in which cells similar to those in the tumors were seen in the blood after death. *Austin Journal of Clinical Medicine* 14: 146-149, 1869.
59. Mocellin S, Keilholz U, Rossi CR and Nitti D: Circulating tumor cells: the 'leukemic phase' of solid cancers. *Trends in Molecular Medicine* 12: 130-139, 2006.
60. Peach G, Kim C, Zacharakis E, Purkayastha S and Ziprin P: Prognostic significance of circulating tumour cells following surgical resection of colorectal cancers: a systematic review. *British Journal of Cancer* 102: 1327-1334, 2010.
61. Alunni-Fabbroni M and Sandri MT: Circulating tumour cells in clinical practice: methods of detection and possible characterization. *Journal of Biological Methods* 50: 289-297, 2010.
62. Allan AL and Keeney M: Circulating tumor cell analysis: technical and statistical considerations for application to the clinic. *Journal of Oncology* 2010: 426218, 2010.
63. Panteleakou Z, Lembessis P, Sourla A, et al: Detection of circulating tumor cells in prostate cancer patients: methodological pitfalls and clinical relevance. *Molecular Medicine* 15: 101-114, 2009.
64. Gordon A, Colman-Lerner A, Chin TE, Benjamin KR, Yu RC,Brent R. Single-cell quantification of molecules and rates usingopen-source microscope-based cytometry. *Nature Methods*. 2007; 4:175–181.16.
65. Dotan E, Cohen SJ, Alpaugh KR and Meropol NJ: Circulating tumor cells: evolving evidence and future challenges. *Oncologist* 14: 1070-1082, 2009.
66. Ring A, Smith IE and Dowsett M: Circulating tumor cells in breast cancer. *Lancet Oncology* 5: 79-88, 2004.
67. Sequist LV, Nagrath S, Toner M, Haber DA and Lynch TJ: The CTC-chip: an exciting new tool to detect circulating tumor cells in lung cancer patients. *Journal of Thoracic Oncology* 4: 281-283, 2009.
68. Nagrath, S., Sequist, L.V., Maheswaran, S., Bell, D.W., Irimia, D., Ulkus, L., Smith, M., Kwak, E.L., Digurmarthy, S., Muzikansky, A., Ryan, P., Balis, U., Tompkins, R.G., Haber, D.A., Toner, M. (2007). Isolation of rare circulating tumor cells in cancer patients by microchip technology. Nature 450.
69. Adams, A.A., Okagbare, P.I., Feng, J., Hupert, M.L., Patterson, D., Gottert, J., McCarley, R.L., Nikitopoulos, D., Murphy, M.C., Soper, S.A., (2008). Highly efficient circulating tumor cell isolation from whole blood and label-free enumeration using polymer-based microfluidics with an integrated conductivity sensor. Journal of the American Chemical Society 130, 10.
70. Gleghorn, J. P., Pratt, E. D., Denning, D., Liu, H., Bander, N. H., Tagawa, S. T., Kirby, B. J. (2010). Capture of circulating tumor cells from whole blood of prostate cancer patients using geometrically enhanced differential immunocapture (GEDI) and a prostate-specific antibody. *Lab on a Chip* 10: 27–29.
71. Pratt, E. D., Huang, C., Hawkins, B. G., Gleghorn, J. P., & Kirby, B. J. (2011). Rare cell capture in microfluidic devices. *Chemical Engineering Science*, *66*(7), 1508–1522.